NASA Technical Memorandum 101613

ASSESSMENT OF COMPUTATIONAL PREDICTION OF TAIL BUFFETING

JOHN W. EDWARDS

JANUARY 1990

National Aeronautics and Space Administration

Langley Research Center
Hampton, Virginia 23665

ASSESSMENT OF COMPUTATIONAL PREDICTION OF TAIL BUFFETING

By
John W. Edwards
NASA Langley Research Center

ABSTRACT

Assessments of the viability of computational methods and the computer resource requirements for the prediction of tail buffeting are made. Issues involved in the use of Euler and Navier-Stokes equations in modeling vortex-dominated and buffet flows are discussed and the requirement for sufficient grid density to allow accurate, converged calculations is stressed. Areas in need of basic fluid dynamics research are highlighted: vorticity convection, vortex breakdown, dynamic turbulence modeling for free shear layers, unsteady flow separation for moderately swept, rounded leading-edge wings, and vortex flows about wings at high subsonic speeds. An estimate of the computer run time for a buffeting response calculation for a full span F-15 aircraft indicates that an improvement in computer and/or algorithm efficiency of three orders of magnitude is needed to enable routine use of such methods. Attention is also drawn to significant uncertainties in the estimates, in particular with regard to nonlinearities contained within the modeling and the question of the repeatability or randomness of buffeting response.

SYMBOLS

d	reference length
f	frequency, Hz.
f_{min}, f_{max}	minimum and maximum frequencies specifying bandwidth for buffeting analysis, Hz.
l	reference length
M	Mach number
N_{st}	number of time-steps for buffet calculation
N_{gp}	total number of grid points, (full-span)
$N_{st/cy}$	number of steps per cycle of oscillation
N_{bod}	number of bodies and surfaces requiring boundary layer grid densities
$N_{gp/wl}$	number of grid points per spatial wavelength

Re	nondimensional Reynolds number
St	nondimensional Strouhal number
T_{cpu}	computer CPU runtime for buffet calculation
T_{tot}	total transient response time for buffet calculation
T_{min}, T_{max}	minimum and maximum periods of oscillation corresponding to f_{max} and f_{min}, sec.
U	velocity, ft/sec
V_{II}	Volume of vorticity convenction Region II (fig. 17)
y_B	buffeting component of structural response parameter
α	angle-of-attack, degrees
δ	boundary layer thickness
Δx, Δy, Δz	grid sizes in the x, y, z directions in Region II (fig. 17)
Δt	computational time-step size for buffet calculation
Λ	wing leading-edge sweep angle, degrees
λ_{min-x}, λ_{min-y}, λ_{min-z}	minimum spatial wavelengths in the x, y, z directions due to flow convection and unsteadiness at f_{max}, ft.
μ	coefficient of viscosity
ρ	density
σ (t)	root-mean-square value of y_B
τ	CFD algorithm speed, μsec per grid point per time step
subscripts	
∞	freestream
lam	laminar
t	turbulent

INTRODUCTION

Current and future military fighters are called upon to perform high angle maneuvers at elevated loading conditions and are experiencing structural fatigue problems due to dynamic buffet loads on aft components of the empennage, in particular the vertical tail. In the past, steady maneuver loads on the aircraft have been predicted based upon a combination of model test data and analysis while dynamic buffet loads could only be estimated from model tests by means of suitable scaling procedures. For the most part, current military aircraft structural designs were accomplished prior to the realization of the extensive high angle maneuvering time the aircraft would accumulate and the resulting damage the structure would sustain. This has led to a desire for improved prediction methods for such dynamic buffet loads, which emerging computational fluid dynamics (CFD) methods might be expected to fulfill. The purpose of this paper is to provide an assessment of the issues involved in such CFD applications and the resources which would be needed to do such computations.

Figure 1, from reference 1, illustrates the concepts of maneuver and dynamic or buffeting components of a representative structural response quantity, $y_B(t)$. The maneuver component is the very low frequency, essentially steady state (D. C.), mean or bias of the signal. All loadings at frequencies below several Hertz are of this nature and include loads such as those due to short period maneuvering. The buffeting component, $y_B(t)$, comprises all of the signal content at higher frequences. A measure of the level of buffet response is the root mean square value of y_B, σ (t). The formula for σ (t) given in the figure is an estimate of the square root of the area under a plot of the power spectral density of y_B versus frequency. Fatigue and accumulated damage predictions based on assumed numbers of stress cycles are directly related to σ and its accurate prediction will be critical. In order to calculate the buffeting structural response it is necessary to predict accurately the unsteady aerodynamic loading (buffet) causing the response. This in turn requires the accurate prediction of the source of the unsteadiness in the airflow. Details of buffet airflows on specific aircraft will be used to illustrate these issues.

Configurations with Stalled Wing Flow.- Figure 2, from reference 12, sketches the buffet flow for the F-15 airplane model. Comments have been added to draw attention to the flow modeling issues. The F-15 wing does not develop intentional vortex lift augmentation and at 22 degrees angle of attack, where vertical tail buffet intensity is greatest, experiences essentially stalled flow over the outer wing panel with some underlying separated flow spilling over the inlet. The wing flow separates in the vicinity of the rounded leading edge in a highly unsteady manner. The subsequent flow convecting downstream past the vertical tails has an overall, average, diffuse vortical flow structure with higher frequency, unsteady swirling flow superimposed. Little is known about the dynamics within the separated region other than steady, average velocities and pressures. Low speed wind tunnel flow visualizations have been made.

Configurations with Intentional Vortex Lift Enhancement.- Figure 3 shows details of the F-18 airplane which was designed to utilize the vortex system developed by the sharp leading edge extension for enhanced stability at high angles. Again, the comments draw attention to flow modeling issues which need to be addressed in any analysis of tail buffeting. The sharp edge forces the flow to separate at angles above a few degrees and the separated flow rolls up to form a vortex which is convected downstream by the mean airflow. For moderate angles, the vortex can remain intact for large distances downstream of the trailing-edge, although it does experience dissipation. For larger angles, the vortex can experience a fluid dynamic instability, termed breakdown or bursting. The bursting location moves upstream with increasing angle, reaching the trailing-edge at an angle $\alpha \cong$ 15-25 degrees. The burst location and the flow downstream is highly unsteady. Little is known about the dynamics within

the burst region other than steady, average velocities and pressures. A few measurements of rms values have been made. Water tunnel, low speed wind tunnel and flight flow visualizations have been made.

The sections to follow will describe: experimental knowledge of vortex-dominated and buffet flows; the fluid dynamic equation levels available for calculation of such flows; estimates of the computational resources needed; and the current status of CFD applications.

VORTEX-DOMINATED AND BUFFET FLOWS

Experimental research in this area has been pursued separately by the aerodynamics and structures communities until recently. Reference 1 summarizes the traditional methods used within the structures community in correlating wind tunnel and flight buffeting response while reference 2 gives a recent assessment of dynamic loads due to flow separation. References 3, 4, 5 report buffet testing on the F/A-18, F-15, and F-111 TACT aircraft. Figure 4, from reference 3, gives buffet pressure frequency responses for the F/A-18 low speed wind tunnel model showing a marked effect of angle of attack upon the frequency for peak amplitudes. Reference 3 also shows this peaking to be a function of airspeed and a key to the tail buffet response via a "tuning" with tail vibration modes. This peaking in strake vortex flows is believed to be due to convection of patches of coherent swirling flow within the burst vortex.

Reference 6 documents recent unsteady pressure and flow visualization tests on an oscillating straked-delta wing model similar in planform to the F-16. Figure 5, from reference 6, summarizes the main features of the two vortex systems (strake and wing vortices) for this model as evidenced by the lift versus angle of attack (AOA). Straked wing configurations like the F-18 and F-16 show the nonlinear vortex lift augmentation seen between 8-18 deg. and the downward break in the lift curve slope caused by the the onset of burst vortex flow over the planform. The maximum normal force coefficient occurs at $\alpha \approx 35$ degrees. At higher angles the flow is fully separated and the value of C_n falls.

While the above research efforts focused on the flow unsteadiness in order to gain understanding of buffeting structural response, parallel efforts by the aerodynamics community have been directed at understanding the physics of separated vortical flows and the gathering of data bases for the validation of CFD codes. The experiments have involved detailed measurements on static, rigid models. Most of this basic research has studied vortex flows about idealized shapes; for instance, highly swept delta wings, sharp leading-edges, etc. Reference 7 summarizes results from the International Vortex Flow Experiment, a joint program studying vortex flow development on a 65 degree cropped delta wing. Tests were conducted between Mach numbers of 0.4 and 4.0. Both sharp and rounded leading-edges were tested for validation of Euler and Navier-Stokes codes, respectively. Also, sweep effects were studied with a 55 deg. swept wing and configuration effects studied with the addition of a canard. Reference 8 summarizes another extensive series of basic wind tunnel tests including an aspect ratio 1.0, 75 deg swept sharp-edged delta wing and a double-delta (80 deg/60 deg) wing. Data bases from these tests include total forces and moments, surface pressures, surface flow visualization and flow field surveys via intrusive pressure probes (which disturb the flow being measured).

Recognizing the need for higher quality flowfield data for code validation, recent tests [9, 10] have utilized nonintrusive three component laser Doppler velocimetry (LDV). Reference 9 gives data for the 75 degree delta wing at $\alpha = 20.5^{o}$. Reference 10 studied in detail the bursting of vortices generated by a 75 degree delta wing. This is also one of the first instances in which primary attention was given to unsteady features; root-mean-square (rms) velocity components are reported in addition to the mean velocities. Reference 10 also focuses attention to the boundary of the burst region just downstream of the burst location as the source of strong fluctuations.

The most recent wind tunnel investigations of vortex flow are beginning to show a merging of the interests of the two communities upon the problem of tail buffeting. Most of the earlier wind tunnel studies of vortex flows are not germane to this issue for a variety of reasons: i.) vortex systems were steady/stable, ii.) unsteadiness was not addressed or measured, iii.) idealized configurations (sharp-edges, highly swept wings, etc) were tested. Reference 11 describes LDV surveys of the flow over a YF-17 model in a low speed wind tunnel. Figure 6, from reference 11, shows mean and rms component velocities for α = 25 deg at a station just ahead of the vertical tail. The strake vortex has burst ahead of this station and the mean streamwise velocity component, u, shows a region of reversed flow centered on the vertical tail location. The maximum rms velocity fluctuations reach levels of approximately 40%, 35%, and 30% for the u, v and w components and mean crossflow angles at the tail vary from -30 degrees at the root to +15 degrees at the tip. The flow over the F-15 aircraft at high angles is different in not containing such high energy concentrated vortices (see fig. 2). Figure 7, from reference 12, shows mean crossflow velocity components at the tail station measured with LDV in a low speed wind tunnel and for α = 20 deg. Mean crossflow angles at the tail varied from +24 deg. at the root to -17 deg. at the tip. Contrary to the burst vortex flow pattern shown in figure 6, no axial reversed flow is seen in the F-15 case. Also, reference 12 comments that hot-wire pressure data shows no high-frequency peaking like that shown in figure 4. However figure 19 of reference 4 indicates the presence of dominant frequencies in the surface pressure spectra.

This survey of wind tunnel testing of vortical and buffeting flows reveals the scarcity of data bases suitable for the validation of CFD calculations of buffeting flows. On the one hand, the aerodynamics community has been heavily occupied understanding and documenting capability for idealized low speed vortex flows. On the other hand, the buffeting and fatigue problems being experienced by current high performance fighter configurations are due to much more complicated flowfields. Vortical and separated flows from multiple aircraft components interact to produce the buffet environment. Also, compressibility and transonic effects at high subsonic speeds and high angles are largely unknown. Figure 8, from reference 13, is an example of the complex surface flow patterns that can be involved in realistic high performance aircraft buffeting. This surface oil flow for a high speed deep buffet penetration condition is a reminder that most of the experimental vortical flow research mentioned above has been for low speed conditions. The appendix to reference 7 discusses recent results on vortex bursting at high subsonic speeds, indicating that there is much that is not known about such flows.

FLUID DYNAMIC MODELING

The dynamics of fluid flows can be studied at many different levels and the complexity of the fluid flow modeling chosen must be carefully chosen to suit the application. Newsome and Kandil[15] provide a concise summary of the governing equations and solution algorithms being applied to vortical flow aerodynamics and also provide a survey of physical modeling issues and computational results. The following discussion will emphasize the resources required for accurate computations. Thus, grid resolution for accurate solutions, the total number of grid points, the allowable time step size and computer speed will be the key players.

Navier-Stokes Equations. The Navier-Stokes (NS) equations for a compressible fluid are derived from the conservation laws of mass, momemtum and energy. This yields five equations relating seven unknowns: density, ρ ; pressure, p; internal energy, e; temperature, T; and three velocity components u, v and w. The two additional relations needed to make the system solvable are provided by an equation of state, such as that for a perfect gas. An additional quantity introduced in the analysis is the coefficient of viscosity, μ. These NS equations describe the unsteady, turbulent motion of fluids. However, the small size of the turbulent eddy flows which they describe and the required grid point

density for accurate resolution preclude their use for flows about complex aircraft geometries. To get around this issue and bring engineering problems such as the aerodynamics of wings and bodies within reach, averaging procedures are used. The small scale, very high frequency eddy flows are eliminated from the modeling by a time-averaging process which produces the "Reynolds-averaged Navier-Stokes (RNS) equations." These RNS equations are capable of describing the steady and unsteady aerodynamic flows encountered in aeroelasticity and buffeting.

In aerodynamic flows, the effects of viscosity are mainly confined to thin regions, termed boundary layers, adjacent to the wings and bodies. Figure 9 shows the growth of a typical boundary layer velocity profile over a flat plate. For attached flows, the boundary layer thickness, δ, is typically only a few percent of the body length and the velocity at the edge of the layer, U_e, is that of the outer (external) inviscid flow. The viscous fluid nearest the surface must satisfy the no-slip boundary condition (U = 0). The viscous sheared flow within the boundary layer is responsible for the production of vorticity which in turn generates lift. The nondimensional Reynolds' number

$$Re = \rho U l/\mu$$

typifies the relative importance of viscosity on the flow. The larger the Reynolds number, the thinner the boundary layer, δ. Typical values of Re, based upon mean aerodynamic chordlength, are less than one million for low speed wind tunnel models and 10-50 million for full scale aircraft flight conditions.

Real boundary layer flows over aerodynamic surfaces contain regions of laminar, transitional and turbulent boundary layers as illustrated in figure 10. Flow near a wing surface near the leading-edge stagnation point is nearly always laminar (purely sheared flow) but usually undergoes transition (i. e. the laminar flow experiences an instability) to turbulent flow in a short distance. The averaging performed by the RNS eqs. treats this addition of turbulence to a laminar flow by introducing an "eddy viscosity" coefficient, μ_t, giving the total viscosity as

$$\mu = \mu_{lam} + \mu_t$$

The introduction of eddy viscosity, μ_t, in the RNS eqs. requires that the effect of turbulence within the boundary layer profile be modeled. This process of turbulence modeling has been the source of extensive research (see reference 14). However, all popular turbulence models have been calibrated against equilibrium, wall-bounded shear flows (fig. 9). At the present time there is no turbulence model that is applicable to a rotational, off-body flow (free shear flow), such as a vortex, either burst or unburst.

The expense involved in RNS eq. calculations is due to the requirement for sufficient grid density to accurately resolve the boundary layer shear flow. This requires 10-20 grid points across the boundary layer. Computer resources are further impacted by the fine grid cells needed by the RNS eqs in the boundary layer since this affects the allowable time step size. To maintain numerical stability with such small grid cells, allowable time step sizes result in several thousands of time steps for each cycle of unsteady motion. This can be as much as an order of magnitude more time steps per cycle than required for the structural dynamic response calculation.

Leading-Edge Vortex Flows. Figure 11 indicates the geometry of concentrated leading-edge vortices generated over a sharp-edged highly swept delta wing at a high angle of attack. The sharp leading-edge causes the flow to separate, creating a thin free shear layer (termed the feeding sheet) through which there are high gradients of the amplitude and direction of the fluid velocity. This viscous sheared region generates vorticity which is fed into the "primary" vortex core above the wing. These concentrated leading-edge vortices can contain high energies, with axial core velocities 2-3 times the freestream velocity. Reference 10 gives details of LDV surveys of such low speed vortices, showing that there is a.) an innermost, rotational, viscous subcore, b.) a middle region of inviscid, rotational flow surrounding the inner core and c.) an outer inviscid, irrotational flow.

Figure 11 indicates a few of the many other details which may be present: reattachment of the flow inboard, followed by spanwise flow across the surface. The reattached spanwise flow on the surface creates its own boundary layer which can itself separate and form a small "secondary" vortex under the primary vortex. On the surface underneath each of these vortices, the high flow velocities induce suction pressures, adding to the lift generated by the wing.

Leading-edge vortices do not persist in the flow indefinitely. Multiple vortex systems, like the two vortices in figure 11, mutually affect each other in downstream regions where they can intertwine with each other as they gradually dissipate due to viscous effects. Also, at higher AOA, the individual vortices experience instabilities or breakdowns. Table I, from reference 15, categorizes regions of vortical flow, terming this region of vortex instability Region III. Figure 12, from reference 16, shows two modes of instability occuring simultaneously on a wing; the "spiral" breakdown on the top and "bubble" breakdown on the bottom. Both forms are highly unsteady both in the location of the burst point and in the flow downstream. Both spiral and bubble vortex breakdown are characterized by an axial stagnation point and a limited region of reversed axial flow. The spiral form of breakdown occurs in three successive stages; a sudden deceleration of the fluid moving along the core, an abrupt kink of the core which then turns with a whirling motion that persists for a few turns and a breakdown to large scale turbulence. Particularly at flight Reynolds numbers, leading-edge vortex breakdown is an unsteady phenomenon characterized by the whirling motion of the spiral form or the oscillation of the bubble form about a mean position in addition to the downstream coherent unsteadiness. Figure 13, from reference 37, gives a conceptual cross sectional schematic of the spiral bursting. The individual coils maintain a large scale coherency for a limited distance and, convected by the freestream flow, will give rise to a characteristic frequency content as observed at a fixed location on the aircraft (e.g. the vertical tail). Such frequency peaks have been noted in buffet tests in the F/A-18 (reference 3) and in low speed wind tunnel tests[10]. Figure 14, from reference 10, shows the region of strong rms velocity fluctuations just downstream of the bursting location and forming a shear layer conical boundary of the region of reversed axial flow. Numerical analysis[10] of high speed film images established that the convection velocity of the spiral cores was close to $U_\infty/2$ and that their frequency was close to 130 Hz., corresponding to a Strouhal number $St = fd/U = 0.7$ (d is the maximum diameter of the recirculating bubble).

Reference 15 states "there is no clear understanding of the mechanisms leading to vortex breakdown. Essential elements seem to be a region of high total pressure loss within the vortex core and an externally imposed axial pressure gradient....despite numerous attempts, a generally accepted theoretical description of vortex breakdown does not exist." Alternative explanations of breakdown mechanisms fall into three groups: hydrodynamic instability theories, stagnation point theories and wave-motion theories. Note also that the properties describing these vortex flows prior to bursting are frequently regarded as having smooth variations. For instance, the free shear layer and rotational vortex cores are regarded as smooth thin sheets and regions. However, upon closer observation more detailed dynamic structures are seen. Figure 15, from reference 17, illustrates intricate details seen in laser light sheet profiles taken before and after the breakdown. The condition is for an 85 degree delta wing at $\alpha = 45$ degrees. The edge of the core and the shear layer exhibit localized patches of vorticity

forming, giving a "lumpy" texture to the flow. What level of detailed simulation of such features is required for accurate buffeting calculations is largely unknown.

This survey of leading-edge vortex flows shows that much is known about such flows for highly swept wings ($\Lambda > 60$ deg.) and, in particular, sharp-edged wings. Much less is known for conditions typical of main wing panels of current fighter aircraft (i.e. $\Lambda \approx$ 40-50 deg. with rounded leading edges). In these cases, it is known that there is no clean pattern of flow developing with increasing angle of attack. Thus, the flow contains features of both leading-edge vortex flow formation and stalled flow. Vortex flow separations may develop over partial regions of the span and be intermittent both in time and spanwise location. Vorticity generation for such conditions will not be easily treated as confined to a single shear layer emanating from a fixed location on the wing as in figure 11.

Euler Equations. If the terms involving the viscous shearing stresses are deleted from the RNS eqs. the inviscid Euler equations result. This model does not require very fine grids near bodies since the viscous boundary layer is not resolved. The no-slip boundary condition is replaced by a condition that the flow direction at the surface be parallel to the surface. These equations are capable of modeling flows with strong shocks and flows containing vorticity (rotational flows). Several issues related to the use of the Euler equations for vortical and buffeting flows which should be understood involve the sources of vorticity production and instability mechanisms in free shear layers and concentrated vortices. The former issue is probably most significant in the "forward" portion of the flow-the forebody and wing leading-edge regions. The latter issue predominates in the downstream region where vortex bursting and large scale swirling motion are encountered. There have been numerous publications showing that the CFD solutions of the Euler equations for sharp leading-edge delta wings do produce vortex flow solutions (for medium sized grids) which are in surprising agreement with important features measured experimentally. Also, medium grid solutions have been shown to predict vortex core axial stagnation points and regions of reveresed flow, thus seeming to simulate vortex bursting. The controversy over the accuracy and convergence of such solutions for sharp and round leading-edge wings is described in detail in reference 15. Reference 18 is representative of Euler equation calculations for such flows while reference 19 concludes that, for blunt/rounded leading-edge wings, Euler equations methods do not give satisfactory results.

STRUCTURAL DYNAMICS SIMULATION FOR BUFFETING RESPONSE

Traditional structural loads analysis methods distinquish between maneuver and dynamic or buffet loads whereas the CFD methods under discussion are, in principle, able to compute the total load directly. This does not come without a price however, since the very low frequency (maneuver) loads must be computed with the same restrictive time step needed for the highest frequency components. Since these low frequency loads can be treated by other methods, a low frequency cutoff limit of 5-10 Hz. will be assumed for buffeting calculations. Also, buffet load spectra typically involve the lower frequency vibration modes so that an upper cutoff frequency may be assumed in the range 40-100 hz. (This paper does not address acoustic resonances/fatigue which occur at higher frequencies and involve local structure panel response.)

The dynamic model of the tail structure will be assumed given by a finite element model (e.g. NASTRAN). The model will be truncated to the 5-20 lowest frequency modes with each mode simulated by an ordinary differential equation of motion. Buffeting response calculations may be performed in several ways. The buffet load environment at the tail is assumed to be calculated by the CFD code as time histories of integrated loads (lift, moment, generalized aerodynamic forces (GAFs)).

- One-way-coupling. Here the modal equations are integrated in time along with the CFD code giving the buffeting structural response and loads. However, it is assumed that the tail motions do not affect the aerodynamic flow environment at the tail. Thus, the buffet loading on the tail is treated as an external forcing function. Since the truncated mode structural equations are linear, frequency response analysis can be used to calculate buffeting response quantities such as power spectral densities and rms values. It is imperative in this approach to account, in some fasion, for aerodynamic damping. Total damping is typically low and the major portion of the buffeting response is concentrated in narrow frequency bands centered on the structural mode resonances. Aerodynamic damping[1] is proportional to dynamic pressure and usually dominates the structural damping. Integrated buffeting response quantities such as rms bending moments are strongly dependent upon the aerodynamic damping. This one-way-coupling method is similar to the Rigid Tail Pressure Method of reference 3.

- Two-way-coupling. In this most complete simulation, the buffet load environment drives the structural equations of motion and the resulting structural motion influences the CFD flow calculation. At each time step, the computational grid about the tail must be moved to maintain alignment with the vibrating tail surface and the updated surface location is used as the new boundary condition by the CFD code.

The two-way coupling method has been used for aeroelastic calculations with CFD codes for attached flow conditions.[38] However, neither of these methods has been demonstrated for buffeting response calculations using CFD codes.

COMPUTATIONAL RESOURCE REQUIREMENTS

We turn now to the estimate of the computer resources which will be required for vertical tail buffeting calculations. The goal will be to obtain at least a ballpark estimate of the computer memory size and job run times. Until recently, the former item was the pacing item in CFD calculations, with the allowable number of grid points being restricted by computer memory sizes. The currently available supercomputers, with memories ranging from 32-256 million words of core memory, have made job run times the pacing item as the estimates below will show.

The CPU run time for a CFD calculation can be estimated from the relation

$$T_{cpu} = N_{st} * N_{gp} * \tau \qquad (1)$$

where

N_{st} = number of time steps in the calculation

N_{gp} = number of grid points

τ = computational time per grid point per time step

Algorithm Speed -The parameter, τ, is a common measure of the speed of an algorithm and typically ranges from 10 - 100 microseconds per grid point per time step. This assumes current computer operational processing speed capability on the order of 250 million floating point operations per second (MFLOPS, typical of the CRAY 2). The value, $\tau = 10$, is typical of "explicit" algorithms which are commonly used for steady-state CFD calculations. Implicit algorithms obtain values of $\tau = 20 - 100$ since they require more complex programming. However, they are favored for time-accurate calculations since they allow larger time steps.. A value of $\tau = 40$ will be assumed herein.

Number of Computational Steps -The parameter N_{st} depends upon the time step size, Δt, and the total real time length necessary for the calculation, T_{tot} (to be distinguished from total CPU run time, T_{cpu}).

$$N_{st} = T_{tot}/\Delta t \qquad (2)$$

The maximum time step size, Δt, is limited by the numerical stability of the algorithm and by the required accuracy for the aerodynamic results. To perform a buffet calculation, the frequency bandwidth of interest must be specified. Let f_{min} and f_{max} designate these frequency limits. Corresponding maximum and minimum periods of oscillation are then given by

$$T_{min} = 1/f_{max} \qquad T_{max} = 1/f_{min}$$

For the F-15, let f_{min} = 10 Hz. and f_{max} = 40 Hz. Now, the time step, Δt, is chosen as

$$\Delta t = T_{min}/N_{st/cy} \qquad (3)$$

where $N_{st/cy}$ is the number of computational steps per cycle of oscillation. For Euler codes this value is set by the required accuracy for the unsteady calculations and is in the range 100-200. For Navier-Stokes codes, smaller time steps are required due to algorithm stability and values of 1000 and higher are needed (due to the much smaller minimum grid size used in order to resolve the boundary layer.). In the examples to follow, $N_{st/cy}$ values of 200 for Euler calculations and 1000 for Navier-Stokes calculations will be used.

The total real time length, T_{tot}, required for buffeting calculations will be set by the number of cycles of oscillation, N_{cy}, at the lowest frequency, f_{min}, in order to obtain converged results.

$$T_{tot} = N_{cy} * T_{max} \qquad (4)$$

Since the buffeting flowfield is inherently nonsteady and nonperiodic, convergence must be measured in some statistical sense such as the attainment of stabilized power spectral densities of selected structural response parameters. A reasonable range of N_{cy} is 10-50. A value of N_{cy} = 10 will be assumed herein.

Summarizing, the total number of steps is given by

$$
\begin{aligned}
N_{st} &= T_{tot}/\Delta t \\
&= (N_{cy} * T_{max})/(T_{min}/N_{st/cy}) \\
&= (N_{cy}/f_{max})/(1/N_{st/cy} * f_{max}) \\
&= N_{cy} * N_{st/cy} * (f_{max}/f_{min})
\end{aligned}
\qquad (5)
$$

For the values selected for the case of the F-15 this gives

N_{st} = (10) * (200) * (40/10) = 8,000 steps (Euler)

= (10) * (1000) * (40/10) = 40,000 steps (Navier-Stokes)

Number of Grid Points - In this section, a first approximation will be developed for the number of grid points needed for a buffeting calculation of the F-15. First, the current CFD experience with solution convergence for isolated wings will be noted. Then attention must be given to the different nature of buffet airflows. These two features will be referred to as "local accuracy" and "remote accuracy." Figure 16, from reference 20, shows the near field of a typical grid used for CFD calculations about an isolated wing. Only the left half-wing is shown since symmetry is usually assumed to cut the total number of grid points required in half. The grid point density is high near the surface of the wing (dark area) where high accuracy is desired for steady calculations, and the density is decreased rapidly away from the wing where lower flow gradients are anticipated and where less accuracy is acceptable. Calculated pressures on the wing surface are used to compute the wing's lift, moment and drag. Thus, the accuracy of these "local" flow quantities is of most interest. On the other hand, for buffet calculations, the accuracy of the flow quantities (e.g. velocities and pressure) at the "remote" tail location will be of paramount interest. For local accuracy with an Euler code on a half-span wing, reference 21 indicates that the following number of grid points results in spatially converged local flow results:

193 grid points in the streamwise direction
33 grid points in the direction normal to the wing
41 grid points in the spanwise direction

The total number of grid points is N_{gp} = 261,000. Reference 20 gives similar information for a Navier-Stokes code calculation:

193 grid points in the streamwise direction
65 grid points in the direction normal to the wing
49 grid points in the spanwise direction

The total number of grid points is N_{gp} = 414,000. Note that the only coordinate direction with significantly higher grid density is that normal to the wing. This is due to the use of the "Thin-Layer Navier-Stokes" equations (TLNS) wherein it is recognized that the viscous shearing forces in the direction normal to the wing predominate in boundary layer flow. Accordingly, the viscous terms in the streamwise and spanwise directions are not treated and no additional grid point density in these directions is called for, leading to a very large reduction in the number of grid points for a viscous calculation. Comparing the two grids, it can be seen that approximately 20 additional grid points in the normal direction are needed to resolve the viscous boundary layer. Thus, the TLNS assumption allows RNS-like results with only a 30-40% increase in cost over Euler codes. We note that there are

approximately 100 streamwise grid points on the wing itself, leading to 100 X 20 X 49 = 98,000 grid points in the boundary layer of the wing. If the use of the thin layer approximation cannot be justified, resolving viscous regions becomes prohibitively expensive. Thus, doubling the resolution for general sheared flows using the RNS equations requires an eightfold increase in the number of grid points (due to increased grid sizes in all three coordinate direction, 2^3).

Turning now to buffet computations, the issues of unsteadiness and the convection of vorticity must be addressed. Now the grid stretching shown in figure 16 cannot be used in the vicinity of the wing-fuselage-tail since remote accuracy is required (the effect of disturbances originating in the wing region must be accurately resolved at the tail). For this purpose, the computational domain will be treated as three regions. In Region I, the boundary layer region of the wing, fuselage and tail, TLNS grid densities will be used to resolve the boundary layers. In Region II, the near-field of the aircraft containing unsteady separated vortical buffeting flow, grid densities adequate to resolve and convect the flow for the frequency bandwidth of interest will be assumed. Region III comprises the outer flow field (inviscid and irrotational) necessary to capture the correct global flow. Thus the total number of grid points is

$$N_{gp} = N^{I}_{gp} + N^{II}_{gp} + N^{III}_{gp} \qquad (7)$$

The number of grid points required for Region III will be a small fraction of the total number of grid points and will be assumed to be N^{III}_{gp} = 50,000. The number of grid points for the boundary layer about each body component will be taken from the TLNS boundary layer grid density cited above:[20]

$$N^{I}_{gp} = (100 \text{ X } 20 \text{ X } 49) \text{ X } 2 \text{ X } N_{bod}$$

$$= 196{,}000 \text{ X } N_{bod}$$

where N_{bod} = the number of component bodies and the factor of two is used for full span modeling.

For a wing-fuselage-tail configuration, N_{bod} = 3 and N^{I}_{gp} = 588,000.

Figure 17 indicates the near-field Region II for the F-15 aircraft where grid density must be adequate to accurately resolve and convect the unsteady features of the flow for the bandwidth of interest. Since most of the energy involved in separated flow buffet is contained in the frequency range of the lower structrual vibration modes, roughly 10-100 Hz., CFD methods must accurately predict the dynamics of the fluid at these frequencies wherever they may occur in the flow. In this section, it will be assumed that the correct amount of unsteady vorticity has already been injected into the flow (e.g. via the viscous boundary layers, Region I). Hence, in Region II the Euler equations will be assumed adequate to accurately convect the vorticity. The following assumptions are made in order to estimate N^{II}_{gp}:

- the near-field Region II shown in figure 17 should have a grid density adequate to resolve buffet frequency components up to f_{max} which will be assumed to be 40 hz.

- fluid disturbances will be assumed to propagate in the streamwise direction at the freestream speed, U_∞. This leads to a minimum spatial wavelength in the x-direction of

$$\lambda_{min-x} = U_\infty / f_{max} \qquad ft/cycle \qquad (8)$$

- to accurately resolve streamwise fluctuations with wavelengths of λ_{min-x}, $N_{gp/wl}$ grid points per wavelength will be assumed. Typical values for $N_{gp/wl}$ are 50-100 ($N_{gp/wl} = 50$ will be assumed herein.)

$$\Delta x = \lambda_{min-x} / N_{gp/wl} \qquad (9)$$

$$= U_\infty / (N_{gp/wl} \times f_{max})$$

- for the large flow angularities found in buffet flows, it will be assumed that the spatial resolution needed for the crossflow directions will be similar to that for the streamwise resolution.

$$\Delta x = \Delta y = \Delta z \qquad (10)$$

- assume a freestream Mach number of M = 0.5, giving $U_\infty \cong 500$ ft/sec.
- for the dimensions shown in figure 17, these assumptions lead to the following grid parameters

$$\lambda_{min-x} = \lambda_{min-y} = \lambda_{min-z} = U_\infty / f_{max} = 500/40 = 12.5 \text{ ft/cycle}$$

$$\Delta x = \Delta y = \Delta z = \lambda_{min-x} / N_{gp/wl} = 12.5/50 = 0.25 \text{ft}$$

and the number of grid points in the near-field Region II shown in figure 17 is calculated to be approximately 1.5×10^6

Thus from eq. (7) the total number of grid points for an F-15 buffet calculation is

$$N_{gp} = 588{,}000 + 1{,}500{,}000 + 50{,}000$$

$$= 2{,}138{,}000$$

Finally, the total CPU run time for one F-15 buffet calculation (full-span), assuming that the TLNS equations are used in Region I and that this determines N_{st}, is estimated to be

$$T_{cpu} = 40{,}000 \times 2{,}138{,}000 \times (40 \times 10^{-6}) / (3600 \text{ sec/hr})$$
$$= 950 \text{ hrs}$$

If an Euler equation calculation is assumed ($N^{I}_{gp} = 0$, no viscous boundary layer, $N_{st} = 8{,}000$) then

$$T_{cpu} = 8{,}000 \text{ X } 1{,}550{,}000 \text{ X } (40\text{X}10^{-6}) / (3600 \text{ sec/hr})$$
$$= 138 \text{ hrs}$$

Equations 1-10 are summarized in Table II. While these extremely long run times would seem quite impractical, they are likely to indicate the range within which solutions with sufficient accuracy to be useful for design decisions will be found. On the one hand, the shorter run time obtained assuming the Euler equations represents an absolute minimum amount of modeling, evidenced by the lack of any physical model for vorticity generation. At the other extreme, the excessive run time of the TLNS example should be capable of being reduced by a number of devices such as; restricting the extent of boundary layer modeling to only those regions essential to simulating unsteady flow separation (wing/strake leading edges, etc), implementing time-accurate local time stepping, and other possibilities.

CURRENT CFD APPLICATIONS AND CAPABILITIES

The above preliminary estimates of computer resource requirements for buffet calculations will now be juxtaposed with the current capabilities of CFD. Representative published applications of CFD methods will be discussed for: complete aircraft configurations near design conditions; vorticity convection; and high angle, steady/unsteady, vortex-dominated cases.

Complete Aircraft Configurations. It is not surprising that the most detailed aircraft geometry modeling has been applied for cases at low angles of attack, near design conditions, where the flow is attached or mildly separated. These conditions are most important in design and the codes can be expected to perform at their best due to good flow quality (steady, attached, thin shear-layers, etc). Thus, indications of the accuracy of results here will help to assess the readiness of the codes for the more demanding buffet conditions. Table III summarizes a number CFD applications for such cases. All of these studies used the TLNS equations and all implemented simple turbulence models. All used convergence acceleration devices (local time-stepping, multigrid, etc) which yield accurate results only for converged, steady flows. Except for reference 23, all made use of assumed symmetry in the flow to reduce by half the grid size (only one-half aircraft model is analyzed). Finally, the codes used in these studies were generally second-order accurate in space and first-order accurate in time.
References 22-24 involve complete aircraft models at transonic speeds while reference 25 involves a detailed forebody/strake model at low speed and high angle. The latter is included due to its complex surface modeling. Fujii and Obayashi[22] modeled the W-18 transport configuration as a wing-fuselage and made calculations for three angles. The overall surface pressures compared fairly well with experiment except in the outboard wing region where elastic deformations were not accounted for. Their numerical algorithm allowed the calculations with 700K grid points to be obtained in 5-6 hours. Flores and Chaderjian's[23] study of the F-16A aircraft is one of the most ambitious applications to date. They modeled the wing, fuselage, tail, inlet, inlet-diverter, and the exhaust nozzle using 27 grid zones for the half-airplane. The flow-through inlet was modeled including power effects. Comparisons with experimental pressures indicated that the wing leading-edge expansion was not adequately resolved and the wing shock location was off by 12% chord. The differences are suspected to be due to insufficient streamwise grid resolution. Doubling the grid size to one million points allowed the calculation of the full-span aircraft at five degrees sideslip angle. This also doubled the

runtime to 50 hours. With regard to buffet calculations, it is interesting to note that the vertical tail tip vortex for this condition dissipated within one tip chordlength due to numerical dissipation (due to grid stretching downstream of the tip). Huband et al.[24] studied the same F-16A (the inlet is faired-over) for a low supersonic Mach number. Their fine grid solution (N_{gp} = 1,241K) occupied 59 million words of memory and required 40 hours of runtime. They obtained favorable agreement with experimental surface pressures but the wing leading-edge suction peaks were not correctly predicted due to lack of numerical resolution.

Thomas et al.[25] studied the vortex flow patterns over the F/A-18 forebody and leading-edge extension (LEX) at low speed and for α = 30 deg. Both laminar and turbulent calculations were made and compared with low Reynolds number, low speed wind tunnel tests and with high Reynolds number flight tests. In terms of surface flow patterns, primary and secondary forebody surface separation lines were well predicted. The laminar calculations (Re = 740K) agreed well with the wind tunnel (Re = 200K) results while the turbulent calculations agreed well with the flight tests (Re = 10^7). The two calculations show significant differences in surface flow patterns indicating the effects of laminar versus turbulent flows. The downstream convection of these vortical flows under buffeting conditions can be expected to lead to transition and turbulence effects on buffet.

In summary, ambitious applications of CFD to complicated aircraft geometries are being performed. Available studies are very encouraging in the overall agreement with experiment. Important areas are also being highlighted where additional grid resolution is needed to achieve local accuracy in such important features as suction peaks and shock locations. Computer runtimes for these cases, where remote accuracy is not required, are in the range of 5-40 hours (half-airplane). It is probable that accurate buffet calculations will require capability such as this for forebody and wing flows in order to generate accurate "starting" conditions for the convecting vortex flows. It is also probable that similar capability will be required to calculate the buffeting response of the tail to the oncoming buffet flow. Indeed, this is likely to be a more difficult problem than the calculation of the "start ing" wing flow due to the turbulent nature of the local flow at the tail (see figure 6).

Vorticity Convection. Any finite difference numerical algorithm must contain a dissipative mechanism for stability. Standard methods involve either the explicit or implicit addition of nonphysical damping terms proportional to a combination of second and fourth spatial differences of the unknown variables. The resulting CFD algorithms have been typically second-order accurate in spatial variation.

For calculations of vortex flows, where the vortex is calculated as a part of the solution and not imposed on the solution, a significant problem is that conventional differencing schemes possess enough artificial dissipation to smear and dissipate the vortex very rapidly. In general, the coarser the finite-difference grid that is used to perform the calculation, the greater the distortion of the vortex. Rai[26] indicates that conventional spatially second-order accurate finite-difference schemes are too dissipative for calculations involving vortices that travel large distances. Studying the model problem of a two-dimensional, crossflow vortex being convected by the freestream, the effect of higher order spatial- and time-accurate differencing was evaluated. A commonly used method (Beam-Warming central spatial differencing and first order accuracy in time) was shown to dissipate more than 20% of its core pressure in only 5 vortex core radii of travel, making it not suitable for such calculations. Increasing the time-accuracy to second order is very effective, decreasing the pressure dissipation to 20% in 45 core radii. Increasing spatial accuracy is also required to further decrease the numerical dissipation: a fifth-order upwind-biased spatial scheme with second-order time-accuracy produced only 3% pressure loss in 45 core radii. To achieve these accuracies, there is also a lower limit on the number of grid points within the vortex core. Reference 26 indicates that an approximate value for this grid density is at least 8-10 grid points per core diameter of the vortex.

No similar study of accuracy and grid density requirements for streamwise vortices, such as leading-edge vortices, has been made. Considering that the initial scale of viscous vortex cores is of the order of several boundary layer thicknesses, and that the location of vortices shed from round leading-edges is not known a priori and changes dynamically as the flow evolves, the implications for the number of grid points required for buffeting calculations are severe. Note that the computational timing estimates in the last section did not include an estimate of any grid points needed for off-the-surface viscous vortex core or shear layer tracking.

High Angle, Vortex-Dominated Cases. Reference 15 surveys applications for this class of flow which is fundamental to buffet flows. Since the flowfields contain more complex fluid dynamics, the body geometries which have been addressed are correspondingly simpler. Hemisphere-cylinders, ellipsoids, cones and simple delta wings predominate and many of the applications are for supersonic/hypersonic speeds which allow the use of simpler numerical algorithms than is the case for subsonic, buffeting conditions. Table IV lists applications relevant to buffet. They are predominately for low speed flows about delta wings. All except that of Hitzel[27] represent applications of the TLNS equations while Hitzel utilizes the Euler equations. Fujii and Schiff[30] used a time-accurate code (first-order in time, second-order in space) while the remaining cases, using convergence acceleration methods, are accurate only for steady flows. Of the TLNS cases, all assumed laminar flow conditions except Vadjak and Schuster[33] who used a turbulence model. Hitzel[27] analyzes the sharp-edged cropped delta-wing described in reference 7 while references 28-32 analyze the 75 deg. sharp-edged delta-wing and the 80-60 deg. round-edged double delta-wing (with variations in sweep and planform) described in reference 8. Vadjak and Schuster[33] give calculations for a sharp-edged generic fighter wing-body configuration. All cases made use of assumed symmetry in the calculations.

- Inviscid Results. Newsome and Kandil[15] discuss at length the issues which have been raised regarding use of the inviscid Euler equations for the calculation of separated vortical flows. Two basic issues are: how does separation occur in an inviscid flow without a clearly defined physical mechanism, and what is the cause of large total pressure losses in the vortex cores computed with Euler codes? For sharp leading-edges, results have been obtained for medium grids which are in fair agreement with measured surface pressures, although they do not show the effect of the secondary vortices. However, cases are shown indicating that these solutions are not converged; solutions on finer grids do not agree as well with experiment. For round leading-edge wings, Euler code results are further affected by the choice of numerical solution algorithm. Hitzel[27] provides a recent summary of such calculations for angles from 10-28 degrees and for several Mach numbers. For α = 24 deg. at M = 0.4 and α = 24, 28 deg. at M = 0.85 the results indicated an unsteady flow structure (although the algorithm used local time stepping) which is argued to be a simulation of vortex breakdown. The lack of a strong Reynolds number effect upon separated leading-edge vortex flows is discussed, as is the lack of strong viscous effects on vortex breakdown. In contrast, compressibility (Mach number) can have a strong influence upon the location of breakdown.

- Viscous Results. The remaining entrees in Table IV are from viscous TLNS codes. Hsu and Liu[28, 29] study the 80-60 deg. double delta wing using a laminar, incompressible code. Reference 28 gives results for α = 12 and 20 degrees and includes variations due to planform and Reynolds number. For the double-delta wing with 955,000 grid points in a "fine" grid, the surface pressure suction peaks under the vortices were not well predicted due to lack of grid resolution but the integrated lift and moment coefficients were very accurate. Reference 29 gives further results for the double-delta wing for angles from 6 - 40 degrees including calculations at α = 35 and 40 degrees indicating unsteadiness and bubble-type vortex breakdown. Whereas the calculations contain reversed axial flow in the burst vortex region starting at x/c = 0.95 for α = 35 deg. and x/c = 0.85 for α = 40 deg., the experimental results show bursting at x/c = 0.6 starting at α = 30 deg. Figure 18, from reference 28, shows the effect of planform

and angle-of-attack upon the vortex flows for angles below bursting. A clear well-organized vortex is indicated for the 60 deg wing which moves inboard with increasing angle. The double-delta wing adds an additional vortex formed at the strake-wing juncture which interacts with the wing vortex, intertwining with it over the wing. With the cropped double-delta wing, an additional vortex appears due to the flow separating from the side edge and at $\alpha = 20$ deg. all three vortices tangle together in the wing-tip region.

Fujii and Schiff[30] present calculations for the same 80-60 deg. double-delta wing using a time-accurate, compressible TLNS code. Results for angles of 12-35 deg. are shown. The lift coefficient agrees well with experiment up to $\alpha \cong 27$ deg. where breakdown occurs. For the 850,000 point grid used the strake vortex at $\alpha = 12$ degrees tended to loose strength rapidly because of numerical dissipation. For 30 and 35 degrees, unsteady vortex breakdowns were calculated. At 30 deg. a bubble-type breakdown was seen at $x/c = 0.85$, while a spiral-type breakdown occurred for 35 deg. at $x/c = 0.6$. Figure 21 of reference 30 shows the time history of the lift coefficient, for the latter case, containing an oscillatory component, presumably due to the spiraling bursted flow, with frequency $f = 0.3\ U / c$. This gives a Strouhal number, based upon maximum burst region diameter, d, of $St \cong 0.1$. These calculations were repeated with the viscous terms deleted in order to simulate the Euler equations and the results differed significantly from the viscous case. For $\alpha = 12$ deg. the two vortices didn't merge over the surface; for $\alpha = 30$ deg. breakdown was not observed; while the $\alpha = 35$ deg. case indicated breakdown. Reference 27 concludes that still better grid resolution is required to obtain quantitative results for such flows.

Thomas et al.[31] studied the 75 deg swept delta wing using a local time-stepping, compressible TLNS code with an 850,000 grid point mesh. Results for angles of 0-40 deg. are shown. The predicted maximum lift coefficient of 1.10 at 35 deg. agrees closely with the measured maximum lift of 1.06 at 33 deg. At 40 deg. a steady, bubble-type reversed flow region (due to breakdown) extending from $x/c = 0.6$ to just downstream of the trailing-edge was observed. The experimental burst location for this condition is $x/c = 0.4$. Detailed comparisons with experiment for $\alpha = 20.5$ deg show good agreement of minimum pressure coefficients under the primary and secondary vortices. Additional calculations for this wing are reported by Taylor et al.[34]. Comparisons with 3-D LDV flowfield measurements for $\alpha = 20.5$ deg. show that the CFD code predicts the physics of the flow well, such as the position of the primary and secondary vortex cores and the position of the secondary separation line. However, differences in the magnitudes of pressure, velocity and vorticity in the region of the primary vortex core were noted. Krist et al.[32] show that these deficiencies are due to grid resolution in that region. Using a grid embedding technique to achieve high grid density there without the necessity of global grid enrichment, it is shown that the deviation from the experimental core velocity approaches zero as the minimum grid spacing in the core region is decreased. Accurate prediction of such vortex core quantities will be needed for accurate buffet predictions.

The final entry in Table IV is that of Vadjak and Schuster[33] who made calculations for a generic fighter configuration consisting of a sharp-edged strake/wing/fuselage. Low speed wind tunnel LDV flowfield data was available and crossflow velocity comparisons for $\alpha = 21$ deg. appear to be good. A bubble-type reverse flow region, indicating breakdown, is observed at approximately $x/c = 0.9$. These comparisons for this high angle, vortex flow case are very noteworthy, particularly due to the complex geometry tested. However, the computational results, obtained with a grid of 101,000 points, cannot be regarded as converged.

In summary, calculations of vortex-dominated flows about simplified highly swept wing geometries at low speeds are available. Early Euler equation results gave encouragement to their use for such flows, but recent detailed studies point to issues regarding their accuracy and convergence for realistic geometries.

The thin-layer Navier-Stokes equations, both laminar and turbulent, are being used. The results capture key features of the flowfield such as primary and secondary vortices and surface pressure details. Indications that vortex breakdown is being simulated have been published. However, all cases surveyed indicated the need for further grid refinement in order to achieve quantitative agreement with experiment. Current grid sizes of 250,000 to 10^6 grid points are being used for half airplane modeling, leading to CPU runtimes of 2-25 hours. These grids are typical of those developed for attached shear flows with the highest grid density near the body. This leads to inadequate density in off-the-body regions where concentrated vortices are located and mesh enrichment methods are being developed to address this problem. A fundamental problem is the lack of any turbulence model designed for dynamic free shear layers.

DISCUSSION

Equation (1) for the total CPU runtime for a buffet calculation can be rearranged to give

$$T_{cpu} = N_{cy} N_{st/cy} \frac{f_{max}}{f_{min}} \tau \left[196{,}000 N_{bod} + \frac{V_{II} N_{gp/wl}^3 f_{max}^3}{U_\infty^3} + 50{,}000 \right] \qquad (11)$$

This expression indicates a strong dependence of T_{cpu} upon f_{max} and U_∞ due to the grid density in the near-field, Region II. For this example, increasing f_{max} from 40-60 Hz increases T_{cpu} by a factor of 3.5 while halving the freestream speed, U_∞, from M = 0.5 to 0.25 results in a six-fold increase in T_{cpu}. The F-15 buffet example indicates that approximately 1000 hours will be required for a TLNS code buffet calculation while a calculation with an Euler code would require 138 hours. The Euler result almost certainly does not have the necessary basic physical modeling and the TLNS runtime is unacceptable for analysis or design applications. In this section, the realism of the TLNS runtime will be discussed, approaches to reducing it will be mentioned, and needed comparisons with experimental buffet studies will be outlined.

TLNS Runtime. Equation 11 assumes complete aircraft modeling and thus makes no assumption of symmetry. This is appropriate since asymmetries in the vortical flows over the wing panels should be anticipated (see Table I). Indeed, it should probably be assumed that the two vortex systems will interact dynamically with each other. The doubling of the runtime due to the doubled grid size must be accepted as necessary.

Equation 11 also assumes that the global time-step is set by the most restrictive criteria - allowable time-step for stability on the smallest grid cell. This restriction is necessary in order to maintain time-accuracy with available codes.

Equation 11 does not include any allowance for grid points to model free viscous shear layers away from the aircraft component surfaces. Regions that might be anticipated to require such extra gridding are: i.) concentrated vortex cores such as those shown in figure 3; ii.) free shear layer surfaces such as those shown in figures 11 and 15 and in the flow separations from rounded leading-edges (figure 2); and iii.) conical surfaces of sheared flow on the boundary of the burst region just downstream of vortex burst locations, see figures 3 and 14. If these regions were steady, straightforward estimation procedures (e.g. 10 grid points across concentrated vortex core diameters, 10-20 grid points in the normal direction through thin free shear layers) seem to indicate modest increases in the number of grid points for a reasonable number of such viscous regions. Unfortunately, these regions are not steady

and so a local grid enrichment strategy will not be successful unless provision is made for moving the dense grid region to track the evolving flow. Also, these regions will not be aligned with the coordinate system in such a way as to take advantage of a "thin-layer" assumption.

If it is assumed that the oncoming freestream flow is steady, there must be a region where unsteadiness first occurs. We can anticipate that the unsteadiness will be due to local instabilities in the flow which are likely to be highly sensitive to a number of parameters. It is also likely that nonlinear mechanisms will be involved, which can lead to extreme sensitivity to initial conditions. This can call for very extensive calculations in order to cover reasonable ranges of conditions or to achieve statistically stable calculations (e.g. stable power spectral density estimates). There is also the possibility of chaotic response, in which there is no repeatability in the response. In this light, the assumption that the number of cycles of oscillation at f_{min} be in the range $10 < N_{cy} < 50$ might be very optimistic.

The CPU runtime estimate for the TLNS equations needs to be reduced by approximately three orders of magnitude (from 1000 hours to approximately 1 hour) before such buffet calculations will be viable. Then the number of cases, the job turn-around time and the computational expense would be at levels that could support efforts leading to reliable engineering tools. These runtime improvements can probably be anticipated due to expected increases in computer speed and memory and increases in algorithm speed and efficiency.

Efficiency Enhancements. There are several direct approaches which should be of use in reducing the CPU runtime estimates. Embedded grids and solution adaptive gridding strategies have already been mentioned wherein the evolving flow solution is searched for regions with high gradients. Additional grid points can then be added selectively in these regions resulting in good accuracy with many fewer total grid points. Another opportunity for reducing the number of grid points is the use of "unstructured grids." Structured grids, like that of figure 16, are constructed along orthogonal coordinate directions, resulting in quadrilateral grid cells. Adding grid points locally to such meshes results in additional grid points being added throughout the mesh. Unstructured grids are typically based upon tetrahedral cell elements and are not arranged along coordinate axes. By giving up the connectivity associated with arranging grid points along coordinate axes, the unstructured approach allows for high densities of tetrahedral cells (whose size can be arbitrarily selected) to model surface geometry in great detail and without requiring global grid enrichment. References 35 and 36 describe the development of these unstructured grid and adaptive grid refinement methods for aeroelastic applications.

The use of multiple CPU processors working on the same problem, termed parallel processing, also has the potential of reducing the computational runtime. Reference 33 reports a speed up of a factor of 10 with the use of vectorization and two parallel processors. Research is also being reported on time-accurate local time-stepping which may yield time savings by circumventing the requirement of using the most stringent allowable time-step size as the global time-step.

While this paper has focused upon finite difference solutions of the flow equations, there are alternative solution methods which might have advantages for buffet calculations. However, only finite difference methods (and the closely related finite volume methods) have advanced to the stage where direct buffet computations appear feasible. Attention should always be given to tradeoffs between highly accurate, expensive solutions and inexpensive, semi-empirical solutions. In this vein, it might be anticipated that somewhat general guidelines will emerge in the course of the computational buffeting studies which will, without doubt, occur.

Experimental Vortex-Dominated and Buffet Studies. This paper has discussed a number of areas in which measurements of vortical and buffeting flowfields are needed in order to validate or verify computational buffeting predictions.

- Unsteady surface pressure time-correlations. Knowledge of the instantaneous surface pressure distribution over the vertical tail is required in order to calculate the tail buffeting response. Time correlated measurements of these pressures are needed along with off-the-surface flowfield measurements in order to begin to understand the interaction between the tail structure and the oncoming buffet flow. This constitutes extremely large data sets and presses the current limits of nonintrusive measurement techniques.

- Basic research into dynamic free shear layer turbulence models is probably vital to achieving buffet prediction accuracies necessary for use in final design.

- Basic research into the instability/breakdown mechanisms of concentrated vortices and free shear layers is needed

- There is a lack of understanding of the flow physics for high angle, high subsonic speed conditions. Off-the-surface transonic features, such as terminating center-line shocks and shock-vortex structures, are known to occur and to have strong influences.

Computational Vortex and Buffet Studies. Among a number of computational issues which could be highlighted, one of the most important is the establishment of required levels of algorithm accuracy and grid densities for nondissipative simulation of streamwise/leading-edge vortices. Another issue which will be difficult to resolve involves the use of computational buffet predictions in the design process. How will such codes be validated? What will be the stated level of accuracy (or uncertainty?) in predicting buffeting response spectra and fatigue lifetimes? Experimental buffet data is usually available in the form of statistical measures. It will be interesting to note the sensitivity and repeatability of the corresponding computed statistical buffet measures to small changes in parameters.

SUMMARY

Computational methods and computer resource requirements for the prediction of tail buffeting have been surveyed. Computational finite difference methods have emerged which can provide accurate solutions of the thin-layer Navier-Stokes equations for flows about complete aircraft. Complex geometries have been modeled for low angles using 500,000 to 10^6 grid points for one-half span and requiring 5-40 hours of computer runtime per case. For higher angle, vortex-dominated flows, computations for idealized geometries using 250,000 to 10^6 grid points for one-half span require 2-25 hours. The existing capability of CFD calculations of vortex-dominated flows offers encouragement with computed primary and secondary vortex locations and surface pressure levels in reasonably good agreement with experiment. Indications that vortex breakdown can be predicted are also encouraging, although there have been no studies to verify the accuracy of computations of buffeting frequency response spectra or spatial correlations. All cases surveyed reported the need for further grid refinement in order to achieve quantitative agreement with experiment. Estimates of the number of grid points and the number the computational steps needed to perform buffet calculations have been developed. For current thin-layer Navier-Stokes codes using a full span grid of over 2×10^6 grid points to model the F-15 airplane, approximately 1000 hours of computer runtime would be required for one buffet response calculation. Factors which could significantly lower or raise this estimate were discussed. Basic experimental studies are needed for the development of free shear layer turbulence models and for understanding of the fluid dynamics involved in the breakdown of concentrated vortices. Research is needed to develop numerical algorithms for convecting vortical flows which are nondissipative or which have controlled levels of dissipation such that accurate buffet calculations will be possible.

It can be anticipated that the three order of magnitude decrease in computer runtime needed to bring computational buffet predictions within reason will be forthcoming due to increases in computer speed and memory and increases in algorithm efficiency. A large unknown factor involves the nature of the origination and evolution of the buffet flowfield. It can also be anticipated that nonlinear fluid dynamic processes will be critical in the accurate simulation of such flows. This may lead to high sensitivity to initial conditions, with the result that estimates of runtimes and the required number of cases may be seriously underestimated.

REFERENCES

1. Huston, W. B.: A Study of the Correlation Between Flight and Wind-Tunnel Buffet Loads. Presented at the Structures and Materials Panel Meeting, April 29-May 3, 1957, Copenhagen, Denmark, AGARD Report III, April-May 1957.

2. Mabey, D. G.: Some Aspects of Aircraft Dynamic Loads Due ot Flow Separation. Royal Aircraft Establishment, Tech. Memo Aero 2110, July 1987.

3. Zimmerman, N. H.; Ferman, M. A.; and Yurkovich, R. N.: Prediction of Tail Buffet Loads for Design Application. AIAA Paper No. 89-1378, presented at AIAA Structures Structural Dynamics and Materials Conference, Mobile, Alabama, April 3-5, 1989.

4. Triplett, W. E.: Pressure Measurements on Twin Vertical Tails in Buffeting Flow. AFWAL-TR-82-3015, Volume I, April 1982.

5. Coe, C. F.; and Cunningham, A. M., Jr.: Predictions of F-111 TACT Aircraft Buffet Response and Correlations of Fluctuating Pressures Measured on Aluminum and Steel Models and the Aircraft. NASA CP 4069, May 1987.

6. Cunningham, A. M., Jr.; den Boer, R. G.; Dogger, C. S. G.; Geurtis, E. G. M.; Persoon, A. J.; Retel, A. P.; and Zwaan, R. J.: Unsteady Low-Speed Wind tunnel Test of a Straked Delta Wing, Oscillating in Pitch. Part I General Description and Discussion of Results, AFWAL TR-87-3098, April 1988.

7. Elsenaar, A.; Hjelmber, L.; Butefisch, K.; and Bannink, W. J.: The International Vortex Flow Experiment. Paper No. 9 in AGARD Conference Proceedings No. 437, Validation of Computational Fluid Dynamics, Volume 1, presented at Fluid Dynamics Panel Symposium, Lisbon, Portugal, May 2-5, 1988.

8. Hummel, D.: Documentation of Separated Flows for Computational Fluid Dynamics Validation. Paper No. 15 in AGARD Conference Proceedings No. 437, Validation of Computational Fluid Dynamics, Volume 2, presented at Fluid Dynamics Panel Symposium, Lisbon, Portugal, May 2-5, 1988.

9. Kjelgaard, S. O.; and Sellers, W. L., III: Detailed Flowfield Measurements Over a 75° Swept Delta Wing for Code Validation. Paper No. 10 in AGARD Conference Proceedings No. 437, Validation of Computational Fluid Dynamics, Volume 2, presented at Fluid Dynamics Panel Symposium, Lisbon, Portugal, May 2-5, 1988.

10. Pagan, D.; and Soligna, J. L.: Experimental Study of the Breakdown of a Vortex Generated by a Delta Wing. Rech. Aérosp. (English Edition) 1986-3.

11. Sellers, W. L., III; Meyers, J. F.; and Hepner, T. E.: LDV Surveys Over a Fighter Model at Moderate to High Angles of Attack. SAE TP Series 881448, Aerospace Technology Conference and Exposition, Anaheim, California, October 3-6, 1988.

12. F-15 Vertical Tail Modifications Project Briefing. School of Aerospace Engineering, Georgia Institute of Technology, presented at Dayton, Ohio, May 17, 1989.

13. Moss, G. F.; and Pierce, D.: The Dynamics Response of Wings in Torsion at High Subsonic Speeds. Paper No. 4 in AGARD-CP-226, Unsteady Airloads in Separated and Transonic Flow, April 1977.

14. Anderson, D. A.; Tannehill, J. C.; and Pletcher, R. H.: Computational Fluid Mechanics and Heat Transfer. Hemisphere Publishing Company, New York, 1984.

15. Newsome, R. W.; and Kandil, O. A.: Vortical Flow Aerodynamics - Physical Aspects and Numerical Simulation. AIAA Paper No. 87-0205, presented at the AIAA 25th Aerospace Sciences Meeting, Reno, Nevada, January 12-15, 1987.

16. Lambourne, N. C.; and Bryer, D. W.: The Bursting of Leading Edge Vortices-Some Observations and Discussion of the Phenomenon. A.R.C. R. and M. No. 3282, 1961.

17. Ng, T. T.; Nelson, R. C.; and Payne, F. M.: Flow Fields Surveys of Leading Edge Vortex Flows. Paper No. 11 in AGARD Conference Proceedings No. 437, Validation of Computational Fluid Dynamics, Volume 1, presented at Fluid Dynamics Panel Symposium, Lisbon, Portugal, May 2-5, 1988.

18. Waner, B.; Hitzel, S. M.; Schmatz, M. A.; Schwarz, W.; Hilgenstock, A.; and Scherr, A.: Status of CRD Validation on the Vortex Flow Experiment. Paper No. 10 in AGARD Conference Proceedings No. 437, Validation of Computational Fluid Dynamics, Volume 1, presented at Fluid Dynamics Panel Symposium, Lisbon, Portugal, May 2-5, 1988.

19. Newsome, R. W.: Euler and Navier-Stokes Solutions for Flow over a Conical Delta Wing. AIAA Journal, vol. 24, no. 4, April 1986.

20. Vatsa, V. N.; and Wedan, B. W.: Development of an Efficient Multigrid Code for 3-D Navier-Stokes Equations. AIAA 89-1791, AIAA 20th Fluid Dynamics, Plasma Dynamics and Lasers Conference, Buffalo, New York, June 12-14, 1989.

21. Anderson, W. K.; and Batina, J. T.: Accurate Solutions, Parameter Studies, and Comparison for the Euler and Potential Flow Equations. Paper No. 15, AGARD 62nd Meeting of the Fluid Dynamics Panel Symposium on Validation of Computational Fluid Dynamics, Lisbon, Portugal, May 2-5, 1989.

22. Fujii, K.; and Obayashi, S.: Navier-Stokes Simulations of Transonic Flows over a Wing-Fuselage Combination. AIAA Journal, vol. 25, no. 12, December 1987.

23. Flores, J.; and Chaderjian, N. M.: The Numerical Simulation of Transonic Separated Flow About the Complete F-16A. AIAA Paper No. 88-2506, presented at the AIAA 6th Applied Aerodynamics Conference, Williamsburg, Virginia, June 6-8, 1988.

24. Huband, G. W.; Rizzetta, D. P.; and Shang, J. J. S.: The Numerical Simulation of the Navier-Stokes Equations for an F-16 Configuration. AIAA Paper No. 88-2507, presented at the AIAA 6th Applied Aerodynamics Conference, Williamsburg, Virginia, June 6-8, 1988.

25. Thomas, J. L.; Walters, R. W.; Reu, T.; Ghaffari, F.; Weston, R. P.; and Luckring, J. M.: A Patched-Grid Algorithm for Complex Configurations Directed Towards the F/A-18 Aircraft. AIAA Paper No. 89-0121, presented at the 27th Aerospace Sciences Meeting, Reno, Nevada, January 9-12, 1989.

26. Rai, M. M.: Navier-Stokes Simulations of Blade-Vortex Interaction Using High-Order Accurate Upwind Schemes. AIAA Paper No. 87-0543, presented at the AIAA 25th Aerospace Sciences Meeting, Reno, Nevada, January 12-15, 1987.

27. Hitzel, S. M.: Wing Vortex-Flows Up Into Vortex-Breakdown. AIAA Paper No. 88-2518, presented at the AIAA 6th Applied Aerodynamics Conference, Williamsburg, Virginia, June 6-8, 1988.

28. Hsu, C.-H.; and Liu, C. H.: Upwind Navier-Stokes Solutions for Leading-Edge Vortex Flows. AIAA Paper No. 89-0265, presented at the 27th Aerospace Sciences Meeting, Reno, Nevada, January 9-12, 1989.

29. Hsu, C.-H.; and Liu, C. H.: Navier-Stokes Computation of Flow Around a Round-Edged Double-Delta Wing. AIAA Paper No. 88-2560-CP, presented at the AIAA 6th Applied Aerodynamics Conference, Williamsburg, Virginia, June 6-8, 1988.

30. Fujii, K.; and Schiff, L. B.: Numerical Simulation of Vortical Flows Over a Strake-Delta Wing. AIAA Paper No. 87-1229, presented at the AIAA 19th Fluid Dynamics, Plasma Dynamics and Lasers Conference, Honolulu, Hawaii, June 8-10, 1987.

31. Thomas, J. L.; Taylor, S. L.; and Anderson, W. K.: Navier-Stokes Computations of Vortical Flows Over Low Speed Aspect Ratio Wings. AIAA Paper No. 87-0207, AIAA 25th Aerospace Sciences Meeting, Reno, Nevada, January 12-15, 1987

32. Krist, S. L.; Thomas, J. L.; Sellers, W. L., III; Kjelgaard, S. O.: An Embedded Grid Formulation Applied to Delta Wings. To be presented at the AIAA Aerospace Sciences Meeting, Reno, Nevada, January , 1990.

33. Vadyak, J. and Schuster, D. M.: Navier-Stokes Simulation of Burst Vortex Flowfields for Fighter Aircraft at High Incidence. AIAA Paper No. 89-2190, presented at the 7th Applied Aerodynamics Conference, Seattle, Washington, July 31-August 2, 1989.

34. Taylor, S. L.; Kjelgaard, S. O.; Weston, R. P.; Thomas, J. L.; and Sellers, W. L., III: Experimental and Computational Study of the Subsonic Flow About a 75° Swept Delta Wing. AIAA Paper No. 87-2425, presented at the AIAA Atmospheric Flight Mechanics Conference, Monterey, California, August 17-19, 1987.

35. Batina, J. T.: Unsteady Euler Algorithm with Unstructured Dynamic Mesh for Complex-Aircraft Aeroelastic Analysis. AIAA Paper No. 89-1189, Presented at the AIAA/ASME/ASCE/AHS/ASC 30th Structures, Structural Dynamics and Materials Conference, Mobile, Alabama, April 3-5, 1989.

36. Batina, J. T.: Vortex-Dominated Conical Flow Computations Using Unstructured Adaptively-Refined Meshes. AIAA Paper No. 89-1816, AIAA 20th Fluid Dynamics, Plasma Dynamics and Lasers Conference, Buffalo, New York, June 12-14, 1989.

37. Payne, F. M.; and Nelson, R. C.: An Experimental Investigation of Vortex Breakdown on a Delta Wing. In NASA CP 2416, Vortex Flow Aerodynamics, Volume I, 1986, proceedings of a conference held at Langley Research Center, Hampton, Virginia, October 8-10, 1985.

38. Bennet, R. M.; Batina, J. T.; and Cunningham, H. J.: Wing Flutter Calculations with the CAP-TSD Unsteady Transonic Small Disturbance Program, AIAA Paper No. 88-2347, AIAA/ASME/ASCE/AHS/ASC 29th Structures, Structural Dynamics and Materials Conference, Williamsburg, Virginia, April 18-20, 1988.

39. Lee, C. C.; Manuel, G. S.; Obara, C. J.; and Wusk, M. S.: Advanced Boundary-Layer Transition Measurement Methods for Laminar Flow Research, ICIASF '89, 13th International Congress of Instrumentation in Aerospace Simulation Facilities, DLR, Gottingen, West Germany, September 18-21, 1989.

40. Wood, R. M.; and Miller, D. S.: Assessment of Prelinimary Prediction Techniques for Wing Leading-Edge Vortex Flows at Supersonic Speeds, Journal of Aircraft, Vol. 22, No. 6, June 1985 pp. 473-478.

Table I

Vortical Flow Regimes as a Function of Angle of Attack (from Reference 15)

Region	Angle of Attack (α)	Flow Characteristics
I	low	Attached flow
II	moderate to high	Stable and symmetric vortical flow
III	very high	Onset of vortex asymmetry and/or vortex breakdown. Nominally steady (lower α), unsteady (higher α)
IV	extreme (up to 90°)	Unsteady diffuse wake possibly with periodic vortex shedding depending upon Re, M_∞, geometry, etc.

Table II

Computer Time Requirements for Buffet Calculations

$$T_{cpu} = N_{st}\, N_{gp}\, \tau$$

$$\tau = 10 - 60\,\mu\text{sec / grid point / time step}$$

$$N_{st} = N_{cy}\, N_{st/cy}\, \frac{f_{max}}{f_{min}}$$

$$N_{gp} = N_{gp}^{I} + N_{gp}^{II} + N_{gp}^{III}$$

$$N_{gp}^{I} \cong (100 \times 20 \times 49) \times 2 \times N_{bod}$$

$$N_{gp}^{II} \cong V_{II} / (\Delta x \cdot \Delta y \cdot \Delta z)$$

$$N_{gp}^{III} \cong 50{,}000$$

$$\Delta x = \lambda_{min_x} / N_{gp/wl} = U_{\infty} / (N_{gp/wl}\, f_{max})$$

$$\Delta y \cong \Delta z \cong \Delta x$$

$$N_{cy} \approx 10 - 50$$

$$N_{st/cy} = \begin{cases} 100 - 200 & \text{(Euler)} \\ \geq 1000 & \text{(RNS)} \end{cases}$$

$$N_{gp/wl} \approx 50 - 100$$

Table III - CFD Applications to Complex Aircraft Geometries

Ref.	Configuration	M	α, deg.	Re, 10^6	N_{st}	N_{gp}	τ, μsec	T_{cpu}, hrs
Fujii[22]	W-18	0.82	2, 4, 6	1.67	3000+	700K	9.5	5-6
Flores[23]	F-16A w/inlet	0.9	6	4.5	5000	500K	36 +	25
Huband[24]	F-16A w/o inlet	1.2	6	12.75	40,000+	1,241K	30 +	40
Thomas[25]	F/A-18 forebody & LEX	0.3	30	0.74 WT 10.0 FLT		300K		

+ - estimated

Table IV - CFD Calculations for Highly-Swept Wings at High Angles of Attack

Ref.	Configuration	Λ, deg	α, deg	Re, 10^6	M	N_{gp}, K	N_{st}	τ, μsec	T_{cpu}, hrs
Hitzel[27]	cropped delta, s, e	65	10,20,24,28* 10-28,24*, 28* 10	1.25	0.4 0.85 1.20	270, 540			
Hsu[28]	delta, r	60	12 (20)	1.3	0	712	700 (1000)	52	7 (10) +
Hsu[28]	double-delta, r	80-60	12 (20)	0.01, 1.3, 100	0	955	700 (1000)	52	10 (14) +
Hsu[28]	cropped double-delta, r	80-40	12 (20)	1.3	0	1021	700 (1000)	52	10 (14) +
Hsu[29]	double-delta, r	80-60	6, 12, 15, 20, 25, 30, 35*, 40*	1.3	0	859	500 (1000)	52	6 (12) +
Fujii[30]	double-delta, r	80-60	6, 12, (30*, 35*)	1.3	0.3	850	1000 (5000)	20	5 (25) +
Thomas[31]	delta, s	75	0-40, 20.5, 40*	0.95	0.3	545	400	40	2.5
Krist[32]	delta, s	75	20.5	0.5	0.3	350 (1000)			
Vadjak[33]	generic wing-body	76-56	10,21*,23,25	1.25	0.3	101	1200		

e - Euler code
s - sharp leading-edge
r - round leading-edge
* - vortex burst/unsteady calculations
+ - estimated

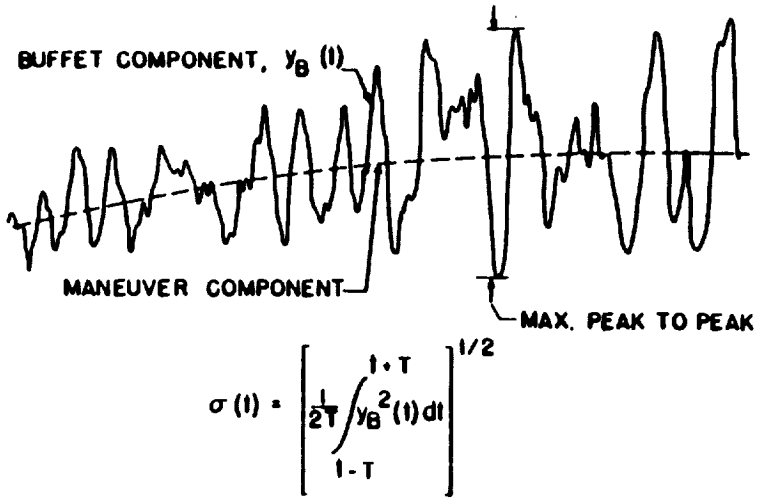

Figure 1. Typical structural response in buffet.

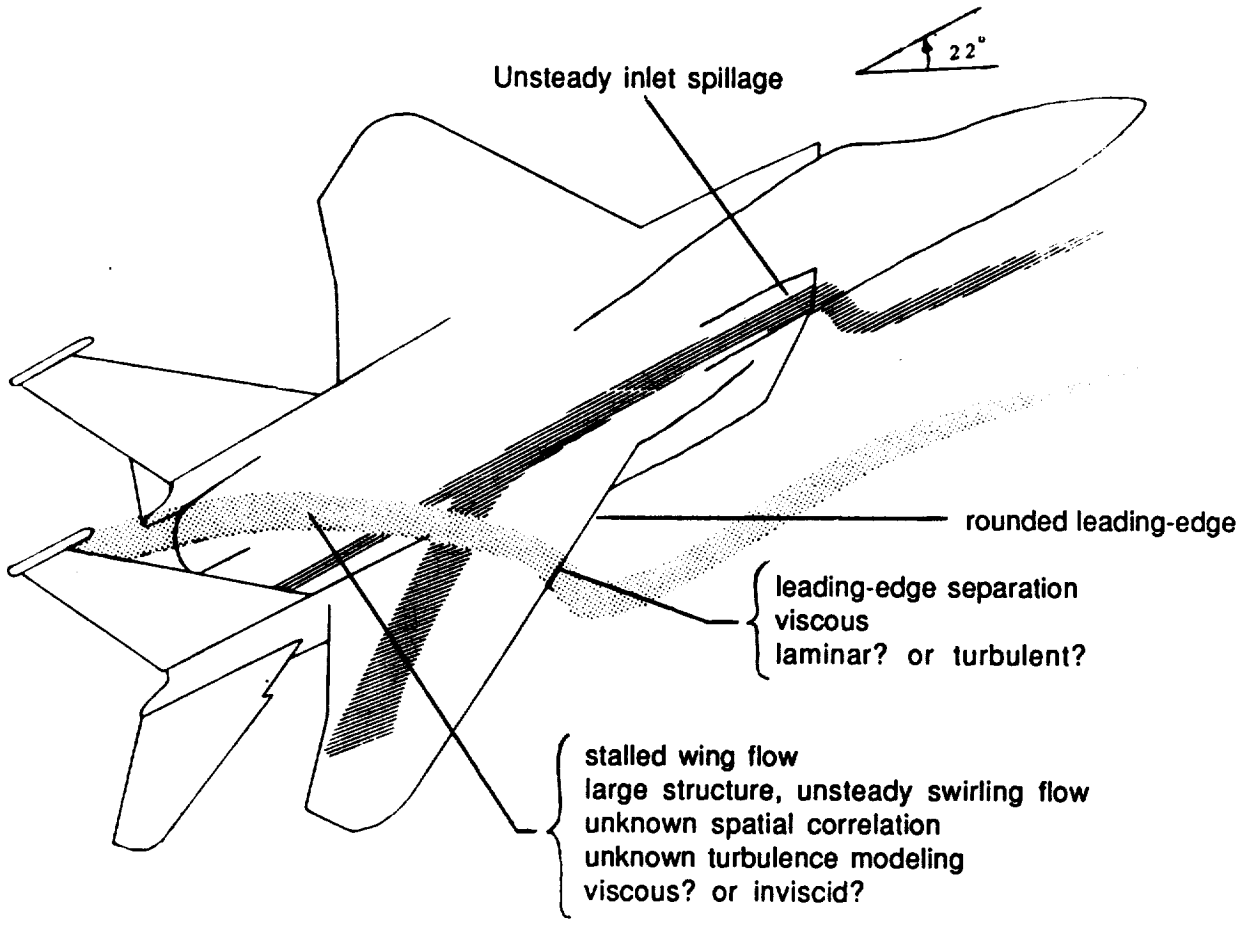

Figure 2. F-15 aircraft in buffeting condition.[12]

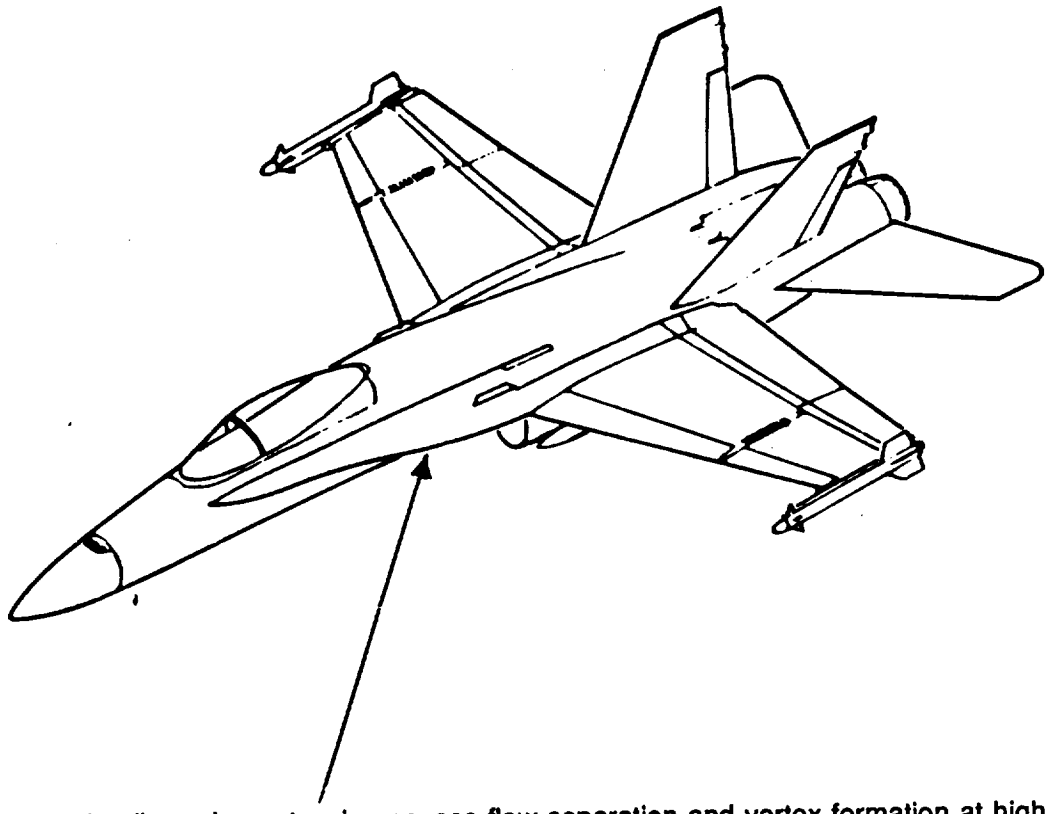

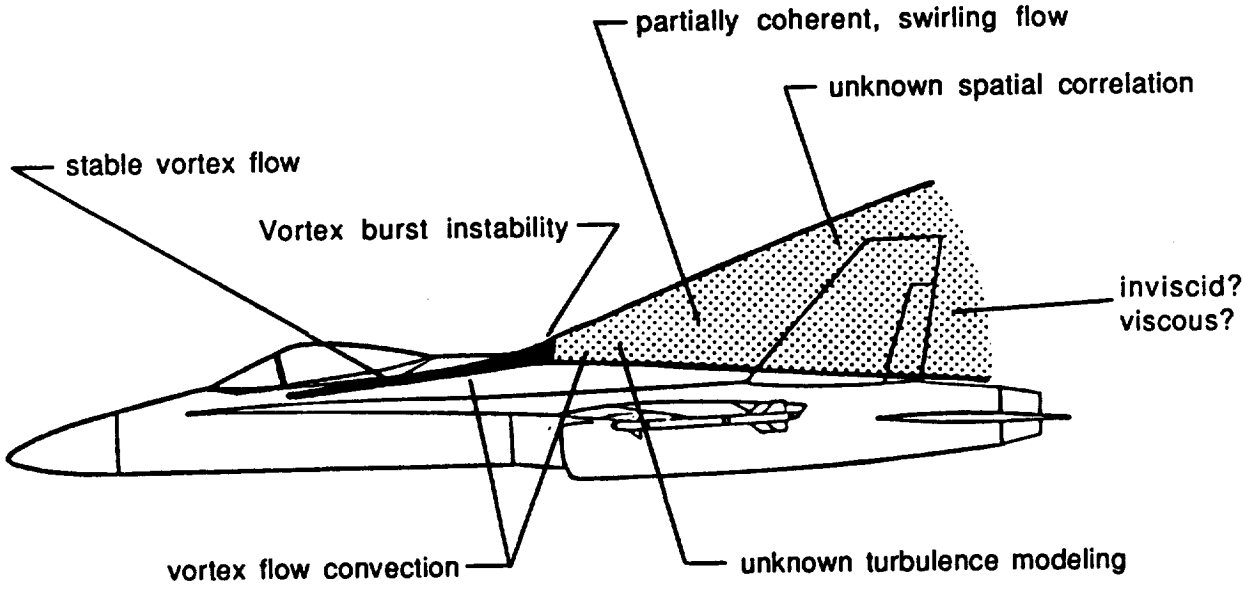

Figure 3. F-18 aircraft at high angle buffeting condition

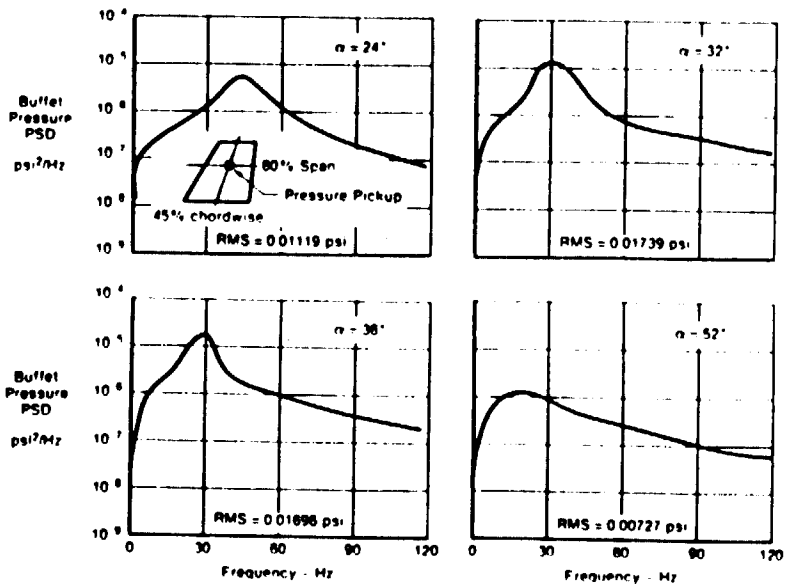

Figure 4. Variation of buffet pressure characteristics with angle-of-attack. (F/A-18 vertical tail, 12% wind tunnel model, V = 81.5 ft/sec, Q = 7.5 psf)[3]

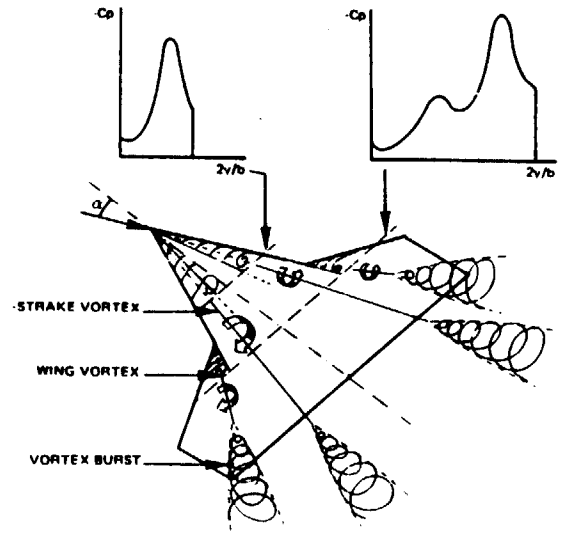

a. Flow over a straked delta wing at high angle-of-attack

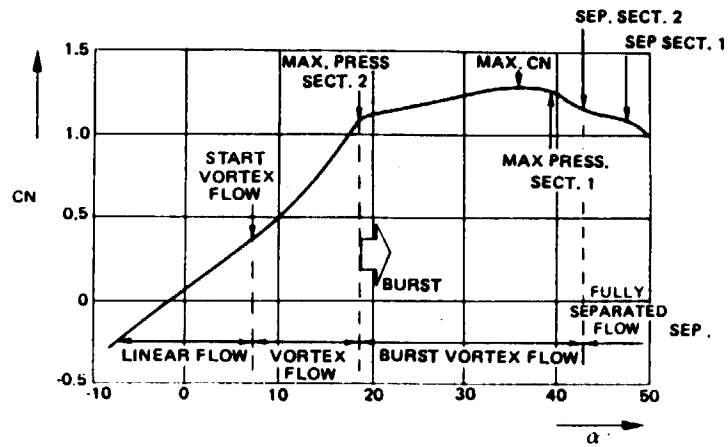

b. Steady normal force coefficient versus angle-of-attack

Figure 5. Vortex flow characteristics for a straked delta wing.[6]

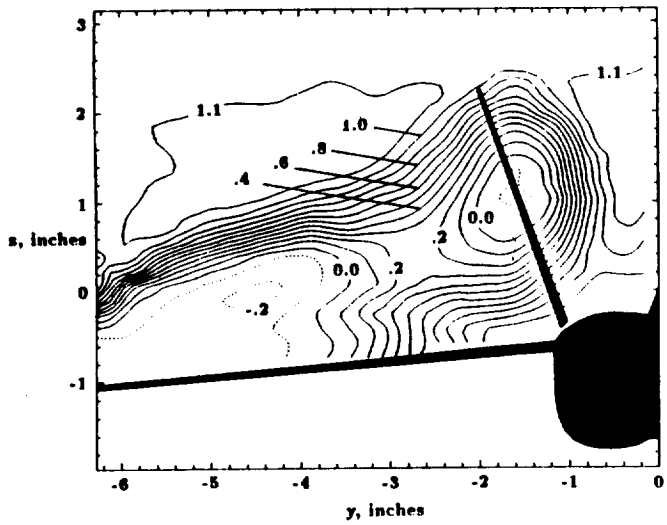

(a) $\overline{u}/V_{\infty}$.

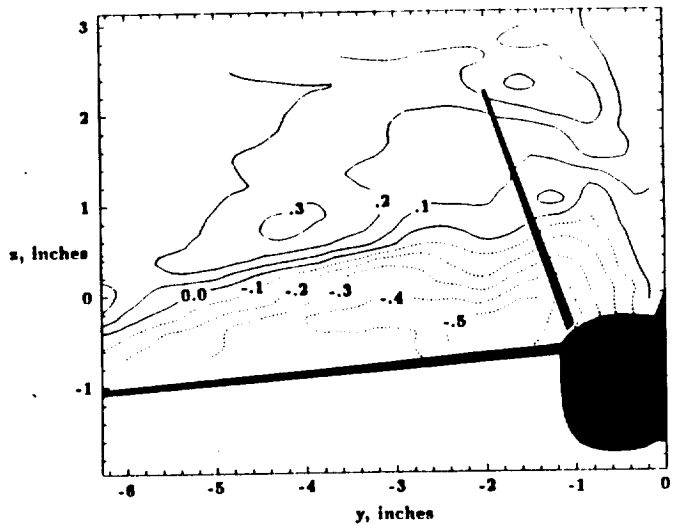

(b) $\overline{v}/V_{\infty}$.

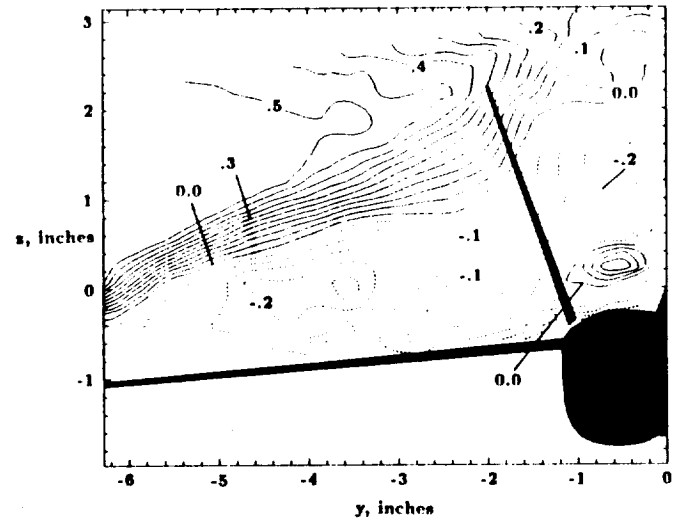

(c) $\overline{w}/V_{\infty}$.

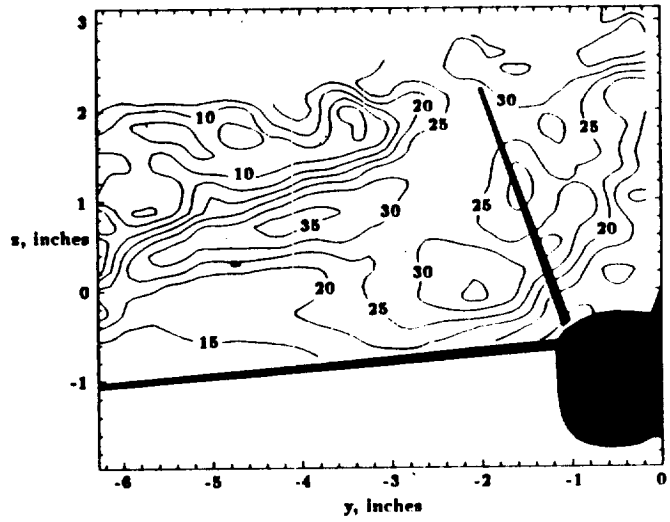

(a) $\tilde{u}/V_{\infty}$, percent.

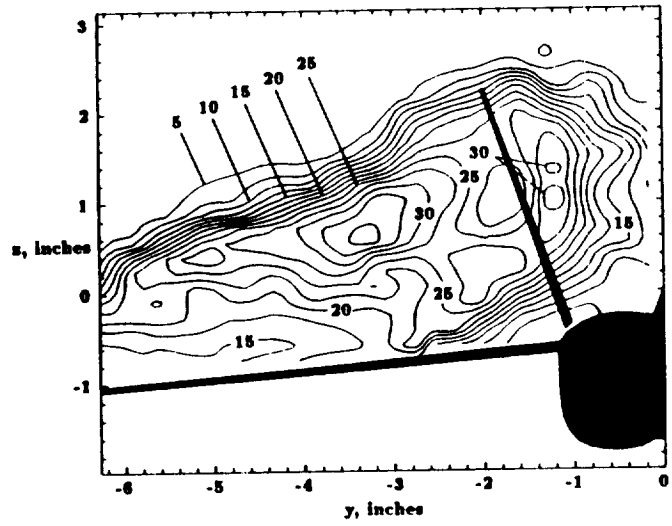

(b) $\tilde{v}/V_{\infty}$, percent.

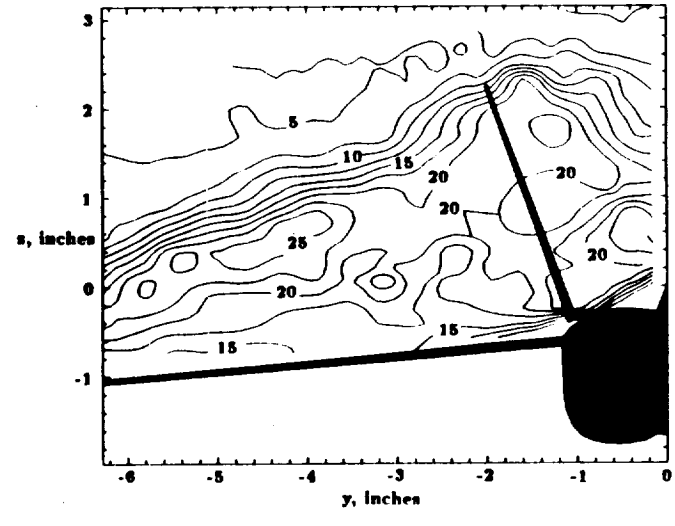

(c) $\tilde{w}/V_{\infty}$, percent.

a. contours of mean velocity

b. RMS velocity contours

Figure 6. Three-component laser velocimetry flow survey for a YF-17 model in a low speed wind tunnel. α = 25 deg, Re = 326,000.[11]

VELOCITY COMPONENTS IN A PLANE UPSTREAM OF THE TAIL

AOA = 20 DEG.

U_∞ = 100 ft/s

1/32 - SCALE

INLET CAPTURE AREA RATIO: 1.0

METHOD: LASER VELOCIMETRY

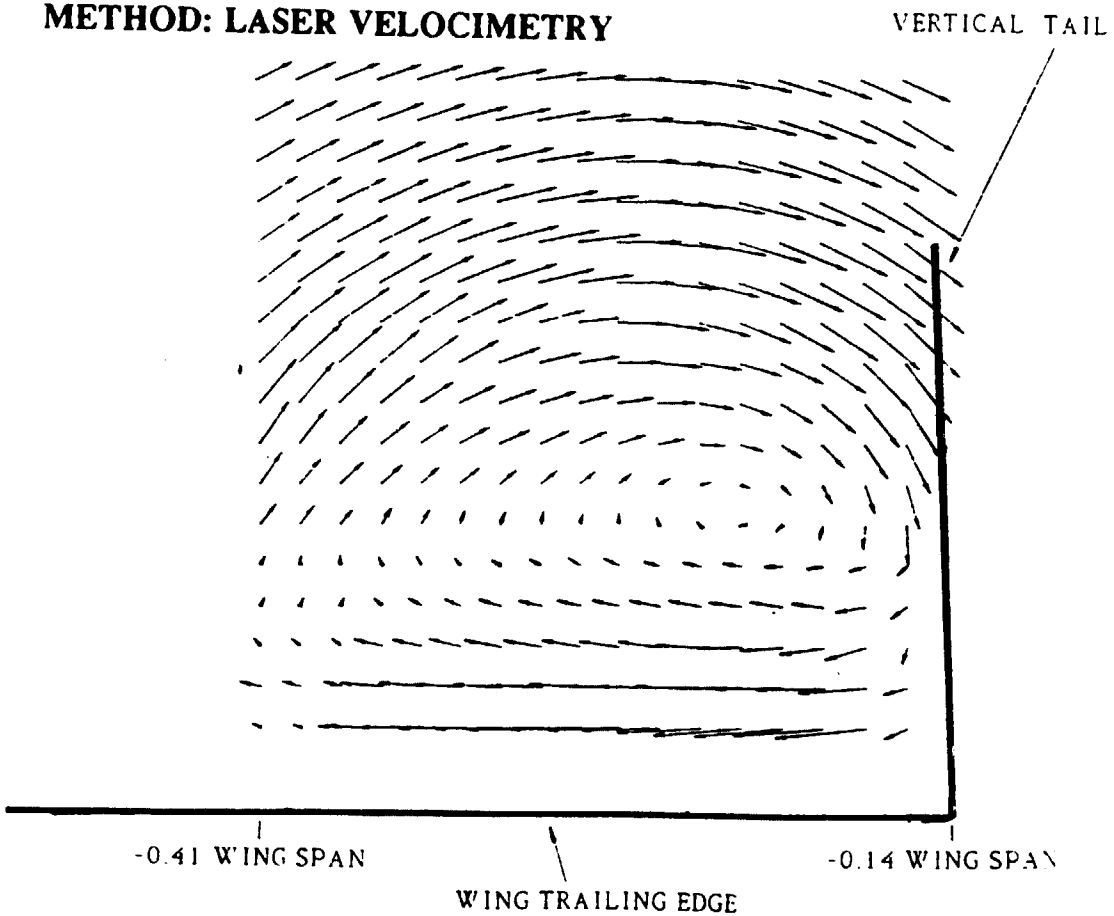

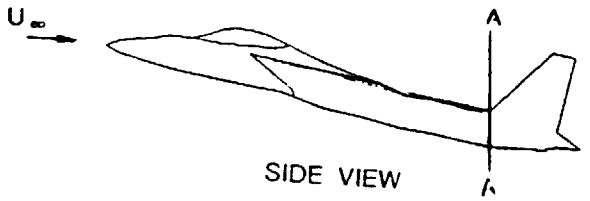

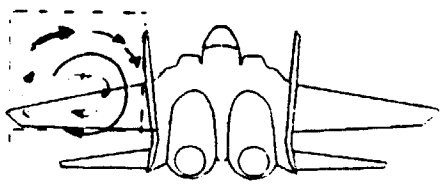

REAR VIEW

Figure 7. Laser velocimetry flow survey of for an F-15 model in a low speed wind tunnel.[12]

ORIGINAL PAGE
BLACK AND WHITE PHOTOGRAPH

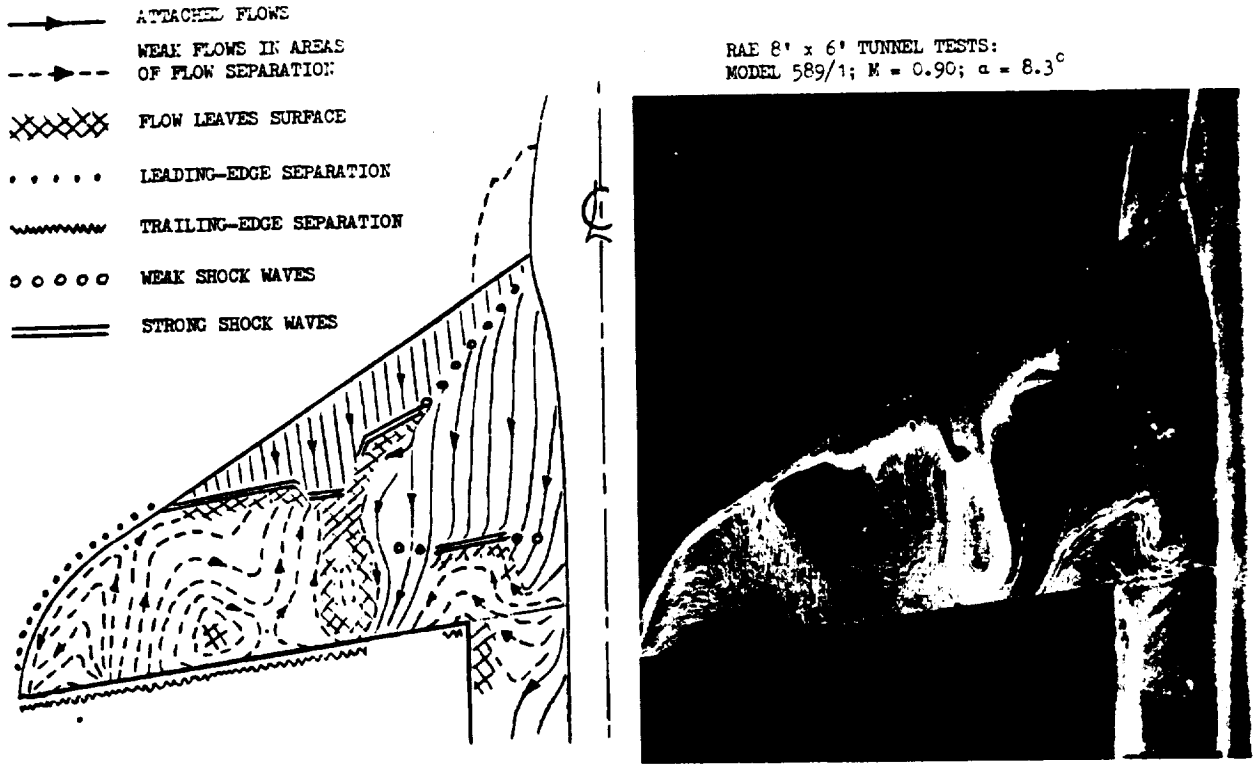

Figure 8. Example of a complex separated-flow situation at deep buffet penetration conditions for a transonic speed.[13]

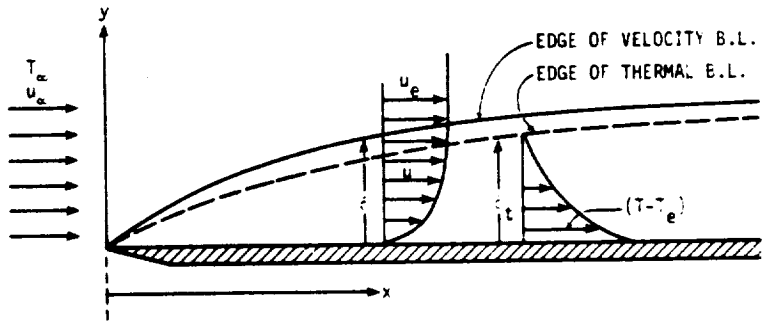

Figure 9. Development of a boundary layer on a flat plate.

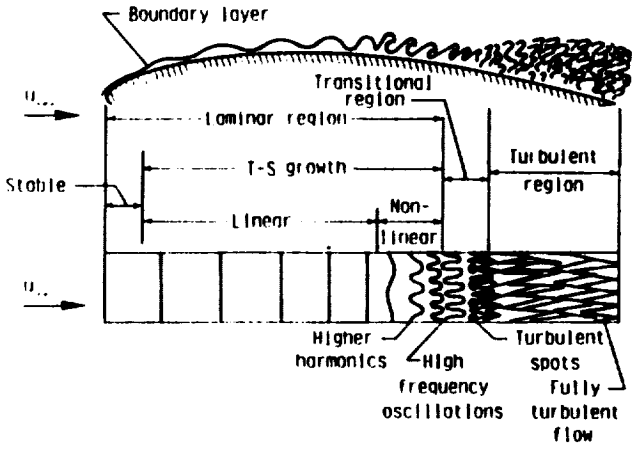

Figure 10. Sketch of boundary layer transition process.[39]

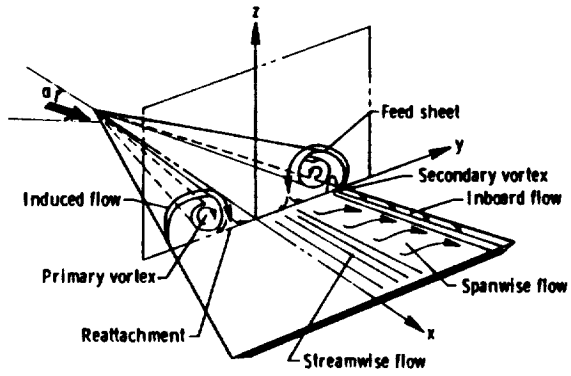

Figure 11. Wing leading-edge vortex flow characteristics.[40]

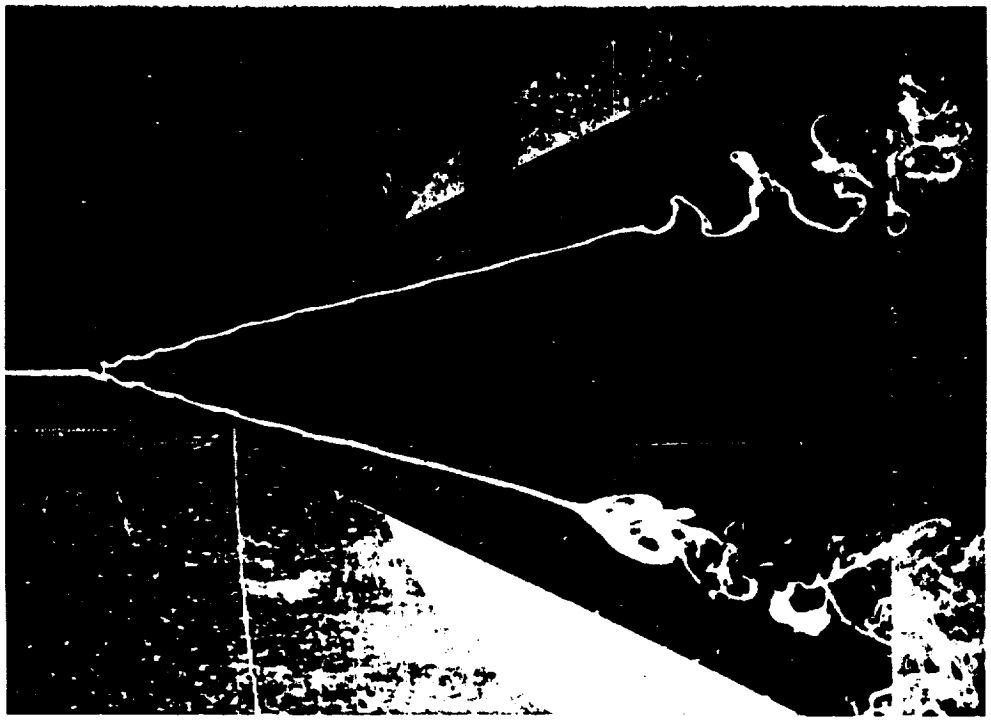

Figure 12. The spiral and bubble modes of vortex breakdown occuring on a delta wing.[16]

ORIGINAL PAGE
BLACK AND WHITE PHOTOGRAPH

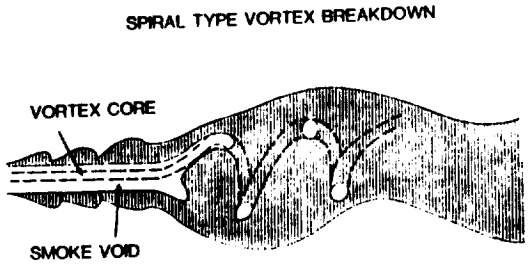

Figure 13. Schematic representation of spiral-type breakdown; longitudinal cross section.[17]

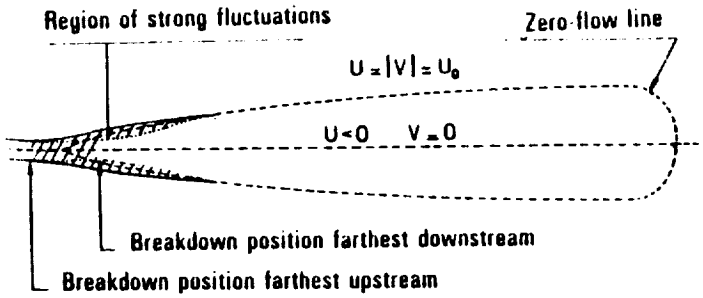

Figure 14. Diagram of vortex breakdown region.[10]

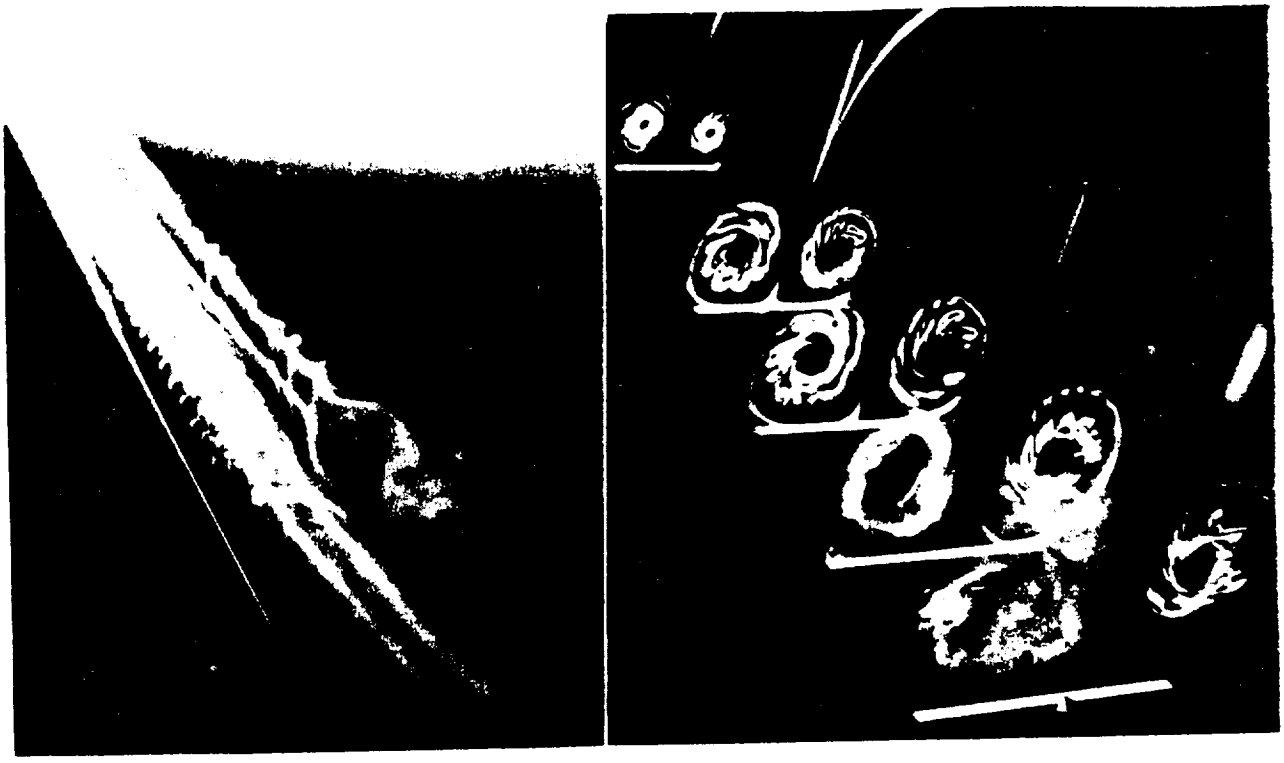

a) Flood lamp

b) Laser light sheet

Figure 15. Smoke flow vizualization of leading-edge vortices on a shart-edged 85 deg. delta wing at $\alpha = 40$ deg.[17]

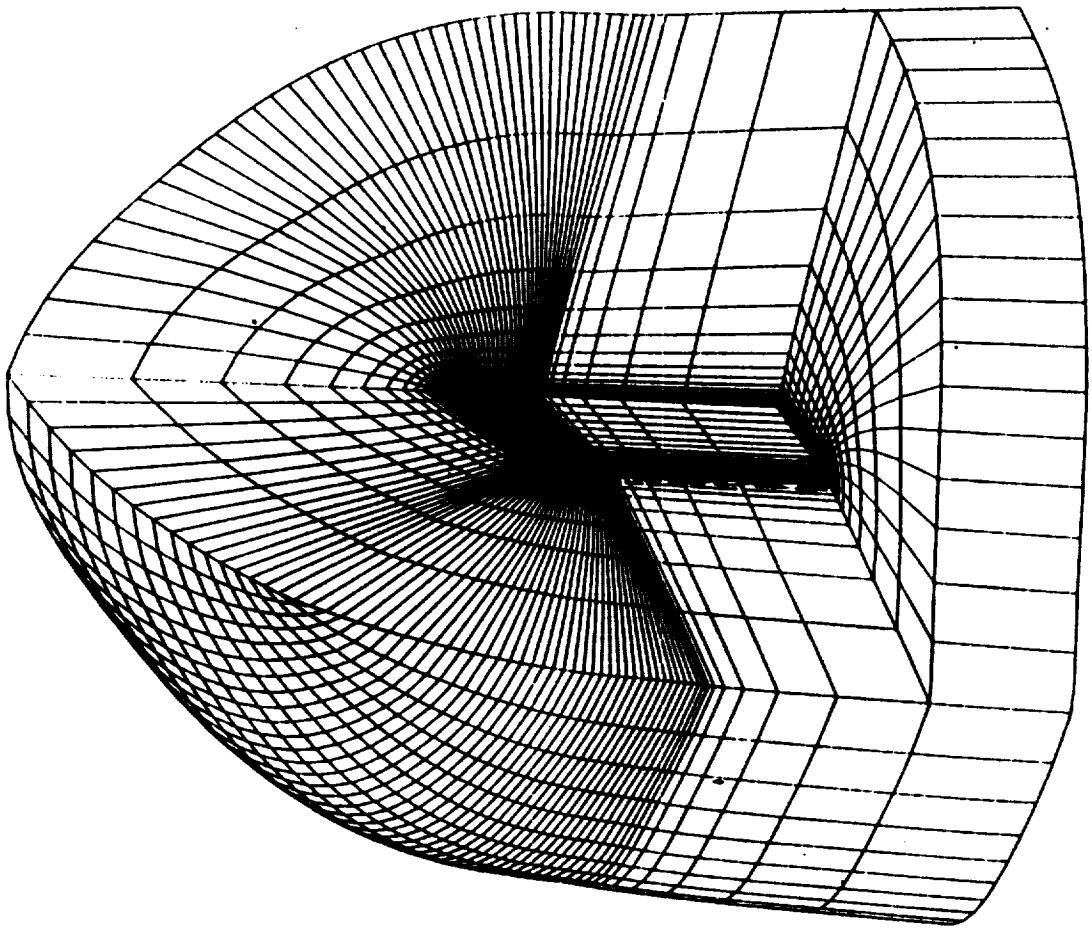

Figure 16. Partial view of computational grid for the ONERA M6 wing.[20]

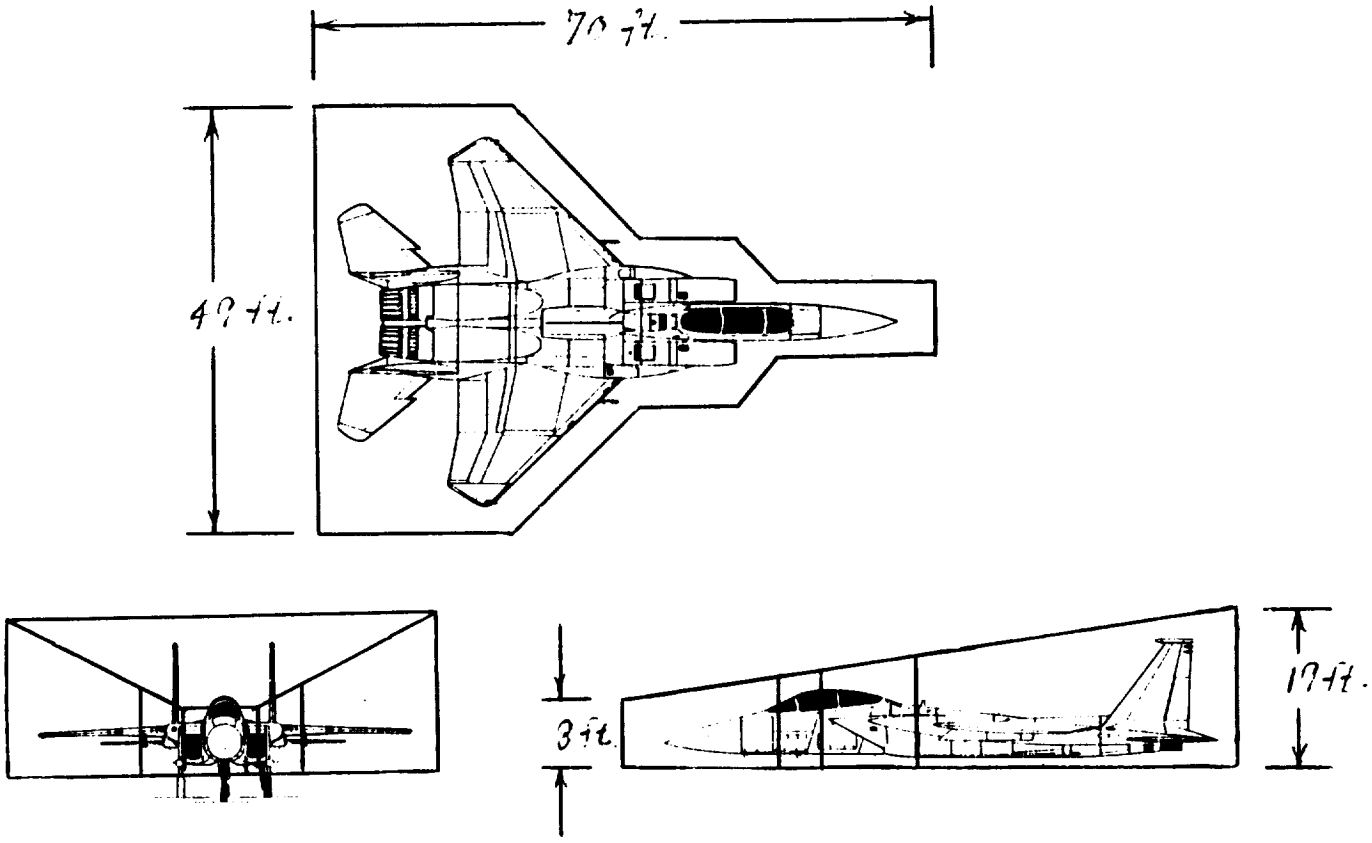

Figure 17. Nearfield volume, Region II, for the F-15 aircraft requiring grid density for accurate vorticity convection calculations.

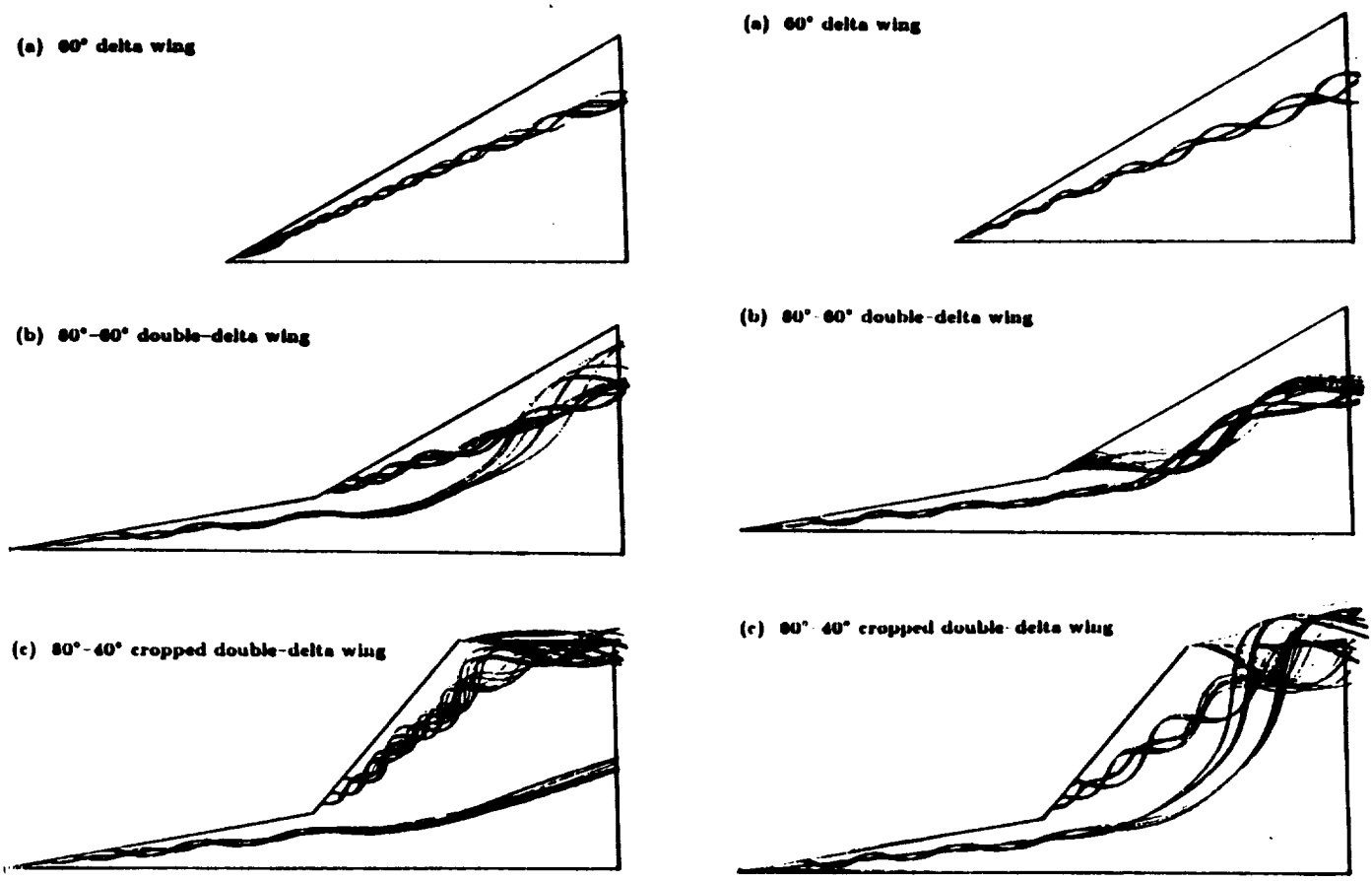

a. α = 12 deg.

b. α = 20 deg.

Figure 18. Top views of off-surface particle traces for three wing planforms.[28]

NASA
National Aeronautics and Space Administration

Report Documentation Page

1. Report No.	2. Government Accession No.	3. Recipient's Catalog No.
NASA TM-101613		

4. Title and Subtitle	5. Report Date
Assessment of Computational Prediction of Tail Buffeting	January 1990
	6. Performing Organization Code

7. Author(s)	8. Performing Organization Report No.
John W. Edwards	
	10. Work Unit No.
	505-63-21-01

9. Performing Organization Name and Address	11. Contract or Grant No.
NASA Langley Research Center Hampton, Virginia 23665-5225	
	13. Type of Report and Period Covered
	Technical Memorandum

12. Sponsoring Agency Name and Address	14. Sponsoring Agency Code
National Aeronautics and Space Administration Washington, DC 20546-0001	

15. Supplementary Notes

16. Abstract

Assessments of the viability of computational methods and the computer resource requirements for the prediction of tail buffeting are made. Issues involved in the use of Euler and Navier-Stokes equations in modeling vortex-dominated and buffet flows are discussed and the requirement for sufficient grid density to allow accurate, converged calculations is stressed. Areas in need of basic fluid dynamics research are highlighted: vorticity convection, vortex breakdown, dynamic turbulence modeling for free shear layers, unsteady flow separation for moderately swept, rounded leading-edge wings, and vortex flows about wings at high subsonic speeds. An estimate of the computer run time for a buffeting response calculation for a full span F-15 aircraft indicates that an improvement in computer and/or algorithm efficiency of three orders of magnitude is needed to enable routine use of such methods. Attention is also drawn to significant uncertainties in the estimates, in particular with regard to nonlinearities contained within the modeling and the question of the repeatability or randomness of buffeting response.

17. Key Words (Suggested by Author(s))	18. Distribution Statement
Unsteady Aerodynamics Aeroelasticity Buffet Vortex flow	Unclassified - Unlimited Subject Category 02

19. Security Classif. (of this report)	20. Security Classif. (of this page)	21. No. of pages	22. Price
Unclassified	Unclassified	41	A03

NASA FORM 1626 OCT 86